Геология и геофизика, 2019, т. 60, № 9, с. 1207—1230

УДК 551.14+553.22(515)

КАК И КОГДА РОСЛО ТИБЕТСКОЕ ПЛАТО?

С. Гийо[1], Ф. Гуссен[1], Л. Эраги[1,2], А. Реплюмаз[1], Ж. де Сигуайе[1], С. Кордье[1]

[1] *University Grenoble Alpes, University Savoie Mont Blanc, CNRS, IRD, IFSTTAR, ISTerre, 38000 Grenoble, France*

[2] *Sorbonne Université, ISTeP, 4 place Jussieu, 75005 Paris, France*

Рост Тибетского плато остается загадкой из-за его размера и большой высоты. На основе синтеза данных по предшествующим коллизиям, палеоальтиметрии, геохимии ультракалиевых лав и их редких мантийных источников в комбинации с реинтерпретацией данных томографии мы предполагаем, что рост Тибета происходил в два основных этапа. Изначально аккреция террейнов Гондваны к окраине Южной Азии, особенно в течение раннего триаса—мелового периода, привела к первому эпизоду роста плато, что оказало влияние на площадь, составлявшую около 2/3 современного плато. Мы предполагаем, что в течение позднего мела кора Тибета достигла мощности около 50—55 км, что является эквивалентным высоте около 2500—3000 м с отдельными формами рельефа, которые могли превышать 4000 м. Еще одним важным последствием этих последовательных аккреций был сильный метасоматизм и смягчение верхней части чехла Тибета. Наблюдаемая в настоящее время низкоскоростная аномалия *P*-волн в центральной части Тибета соответствует не температурной, а вещественной аномалии. Начиная с 50 млн лет назад встречное движение Индии и Азии, которое оценивается в 1000 км со стороны Тибета, привело к сокращению плато примерно на 40 %. Мы предполагаем, что это дополнительное укорочение, которое привело к современной мощности земной коры в 70 км и средней высоте 4800 м, компенсировалось реактивацией континентальных слэбов вдоль предыдущих сутур и равномерным укорочением коры.

Континентальная субдукция, метасоматизированная литосфера, реология, протоплато, Тибет.

HOW AND WHEN DID THE TIBETAN PLATEAU GROW?

S. Guillot, F. Goussin, L. Airaghi, A. Replumaz, J. de Sigoyer, and C. Cordier

Due to its size and high altitude, the growth of the Tibetan Plateau remains an enigma. Based on a synthesis of anterior collisions, paleoaltimetric data, geochemistry of ultrapotassic lava and their rare mantle enclaves, combined with a reinterpretation of tomographic data, we suppose that Tibet's growth took place in two main stages. Initially, the accretion of Gondwana terranes to the margin of South Asia, especially during the Early Triassic–Cretaceous period, resulted in the first episode of plateau growth, which affected an area of about 2/3 of the current plateau. We suppose that during the Late Cretaceous, the Tibetan crust reached a thickness of about 50–55 km, which is equivalent to an altitude of about 2500 to 3000 m, with local landforms that could have exceeded 4000 m. Another important consequence of these successive accretions was a strong metasomatism and a softening of the upper part of the Tibetan cover. The *P* wave low-velocity anomaly currently observed under the central part of Tibet would correspond not to a temperature anomaly but to a composition anomaly. From 50 Ma onwards, the convergence between India and Asia, estimated at about 1000 km on the Tibetan side, led to a shortening of the plateau by about 40%. We suppose that this additional shortening, which has led to the current thickness of the Earth's crust of about 70 km and an average altitude of 4800 m, has been compensated by the reactivation of the continental slabs along the previous sutures and by the homogeneous shortening of the crust.

Continental subduction, metasomatized lithosphere, rheology, protoplateau, Tibet

INTRODUCTION

The orogenic plateaus, covering a surface of thousands of square km, occupy a special place in the plate tectonics. In contrast with oceanic domains and subduction zones, where the deformation is localized along the 10 to 100 km wide oceanic ridges and oceanic trenches respectively, the deformation of orogenic plateaus is distributed over thousands of kilometers, making the definition of plate boundaries more complex.

The processes that control the transition from a narrow orogenic belt to a plateau are poorly understood. Two different views are proposed: (1) a deformation localized along reactivated suture zones and/or lithospheric strike-slip faults that migrates towards the margins of the plateau with a gradual transfer of compressive constraints (Tapponnier et al., 2001) and (2) a distributed deformation throughout the plateau followed by the delamination of the lithospheric root (Molnar et al., 1993). Among the plateaus on the Earth, the Tibetan Plateau is not only the largest but also the most enigmatic.

✉e-mail adress: Stephane.Guillot@univ-grenoble-alpes-fr

DOI: 10.15372/GiG2019126

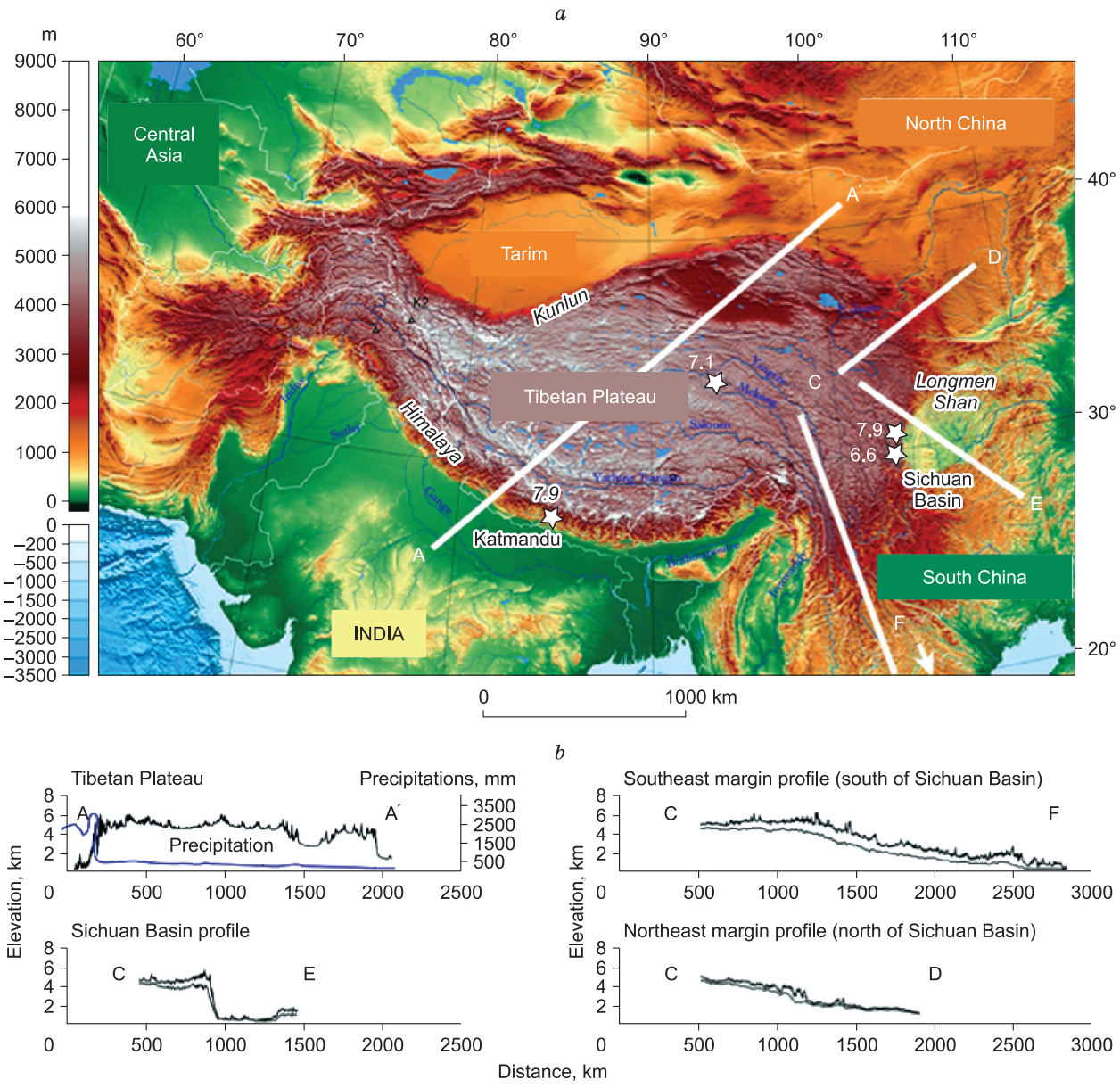

Fig. 1. *a*, Topographic map of the Tibetan Plateau and adjacent regions based on GLOBE and ETOPO1 DEMs.

The stars correspond to the location of recent large recent earthquakes. *b*, Topographic profiles. The upper curves correspond to the maximum altitude, the lower curves correspond to the mean altitude.

At the boundary between the Indian subcontinent and Asia, the Tibetan Plateau forms a relatively flat area of over 2 million km^2 with an average altitude of 4500 m. The topographic gradients at its southern, eastern and northwestern margins (Himalaya, Longmen Shan and Kunlun, respectively) are extreme: altitudes fall from 4500–5000 m within the plateau to less than 1000 m over a distance of 200 km (Fig. 1).

When compared to three of the major mountain ranges in the world, the Andes, the

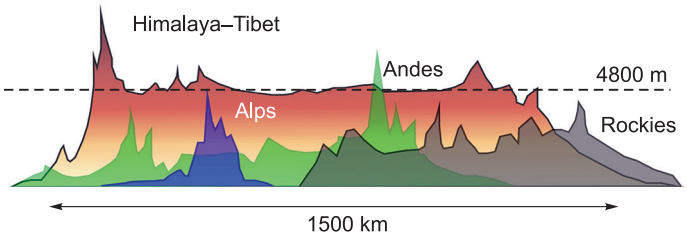

Fig. 2. Topographic profiles of four major mountain ranges (ETOPO1 DEMs).

The dashed line corresponds to the average altitude of the Tibetan Plateau.

Rocky Mountains and the Alps, the Himalaya–Tibet orogen is not only wider, but significantly higher in its average altitude (Fig. 2). A correlation can be established between the size of mountain ranges and their geodynamic evolution. The construction of a small mountain range like the Alps, for example, was triggered by the closure of only one oceanic domain, while the Rocky Mountains resulted from the successive accretion of terranes since the late Paleozoic to the present-day subduction of the Pacific Plate (Price, 1981). The Andes, half in size only to the Himalaya–Tibet system have also been built through the accretion of terranes from the Paleozoic to the present-day as well as by the active subduction of oceanic plates to the west and the continental subduction of the Brazilian craton to the east (Cordani et al., 2000).

As the other major mountain ranges, the Tibetan Plateau is made up of continental terranes, progressively accreted at the southern margin of Eurasia throughout the Mesozoic and the Cenozoic (Yin and Harrison, 2000). However, whereas the successive episodes of accretion were responsible for the construction of a Proto-Tibet, or if the plateau is the result of the sole collision between India and the southern margin of the Asian belt still remains unclear. Were the intra-Tibet suture zones reactivated during the Cenozoic, resulting in the localization of the deformation? Or does the Tibetan Plateau experience an homogeneous thickening of the crust and the lithosphere? In this paper we discuss the pre-Himalayan history of Tibet and its Cenozoic evolution to propose a model for the formation of the Tibetan Plateau. We particularly focus on the paleoaltitudes, tectonic and magmatic evolution. Using geophysical and magmatic data, the rheological behavior of the Tibetan lithosphere will also be discussed. Finally, we will propose a scenario that attempts to take account of all the available constraints.

THE COMPOSITE STRUCTURE OF THE TIBETAN PLATEAU AND THE PRE-CENOZOIC HISTORY

It is widely documented that the Tibetan Plateau is constituted of continental terranes progressively accreted at the southern margin of Eurasia throughout the Mesozoic, from north to south: the Qilian Shan, the Qaidam Basin, the Songpan–Ganze, the Qiangtang, and the Lhasa terranes (Fig. 3). It is noticeable that the India–Asia collision built Tibet but also reactivated further north the Central Asian Orogenic belt from Baikal to the Stanovoi Range in Siberia (Molnar and Tapponnier, 1975; Dobretsov et al., 1996).

The northeastern active front of the Tibetan Plateau corresponds to the Nan Shan thrust, in the prolongation of the active Altyn Tagh fault. It marks the thrusting of the Qilian Shan over the southern margin of the North China Craton. South of that, the Qilian Shan consists of a fold-and-thrust belt of accreted Ordovician to Late Devonian arc systems (Yin and Harrison, 2000), imbricated with Precambrian continental slivers from the North China craton.

The south Qilian Suture marks the major boundary with the Qaidam terrane. The Qaidam basin occupies most of this terrane: it is the largest intermountain depression inside Tibet, having an average elevation of ~ 2000 m lower than the surrounding area. It preserves a complete 10 to 15 km-thick series of Cenozoic detrital sediments (Métivier et al., 1998). The basin has progressively expanded eastward since the initiation of the subsidence during the Late Cretaceous–early Eocene (Wang et al., 2006; Yin et al., 2008). An early Palaeozoic arc, superimposed by the two Permian–Triassic Kunlun batholiths, underlies the southern portion of the Qaidam terrane, defining the South Kunlun suture. Three almost complete ophiolitic sequences with Cambrian, Carboniferous and Permian–Triassic ages have been identified within the Kunlun suture (Yang et al., 1996). The oldest two relate to the very long Paleozoic history of the southern margin of the Eurasian continent (e.g., (Wu et al., 2016)), while the Permian–Triassic ophiolite probably represents the relicts of the northern margin of the Paleo-Tethys that had closed between 260 and 210 Ma along a north-dipping subduction (Yin and Harrison, 2000; Roger et al., 2010).

The Songpan-Ganze terrane occupies a large portion of the central Tibetan Plateau and extends eastwards in the Longmen Shan (Fig. 3). Westward, this terrane is bounded and offset by the left-lateral strike-slip Altyn Tagh fault and the dextral Karakorum strike-slip fault. The Songpan-Ganze terrane is a peculiar geological area since it is characterized by a monotonous 10 to 15 km thick Triassic flysch (e.g., (Calassou, 1994)). The flysch complex was significantly deformed during the Late Triassic collision between the South and North China cratons. P-wave velocities ranging from 6.6 to 6.9 km/s indicate an intermediate continental crustal composition rather than an oceanic one (Karplus et al., 2011). South of the Songpan-Ganze, the Jinsha suture marks the boundary with the Qiangtang terrane and the closure of the southern margin of the Paleo-Tethys. The ages of the ophiolites along the sutures of Jinsha and Ganze-Litang range from 292 to 232 Ma (Liu et al., 2016). The magmatic arcs of Yushu and Yidun record the two-phase closure of the Paleo-Tethys during the Triassic, one of which occurred between 244 and 224 Ma and the other between 219 and 195 Ma, ending with the southward subduction of the Songpan-Ganze terrane (de Sigoyer et al., 2014; Yang et al., 2014).

The wide Hoh Xil Basin (83,000 km^2) overlies the central and western parts of the Songpan-Ganze terrane. It is bounded to the south by the Tanggula Shan and to the north by the Kunlun Shan. In the center of the

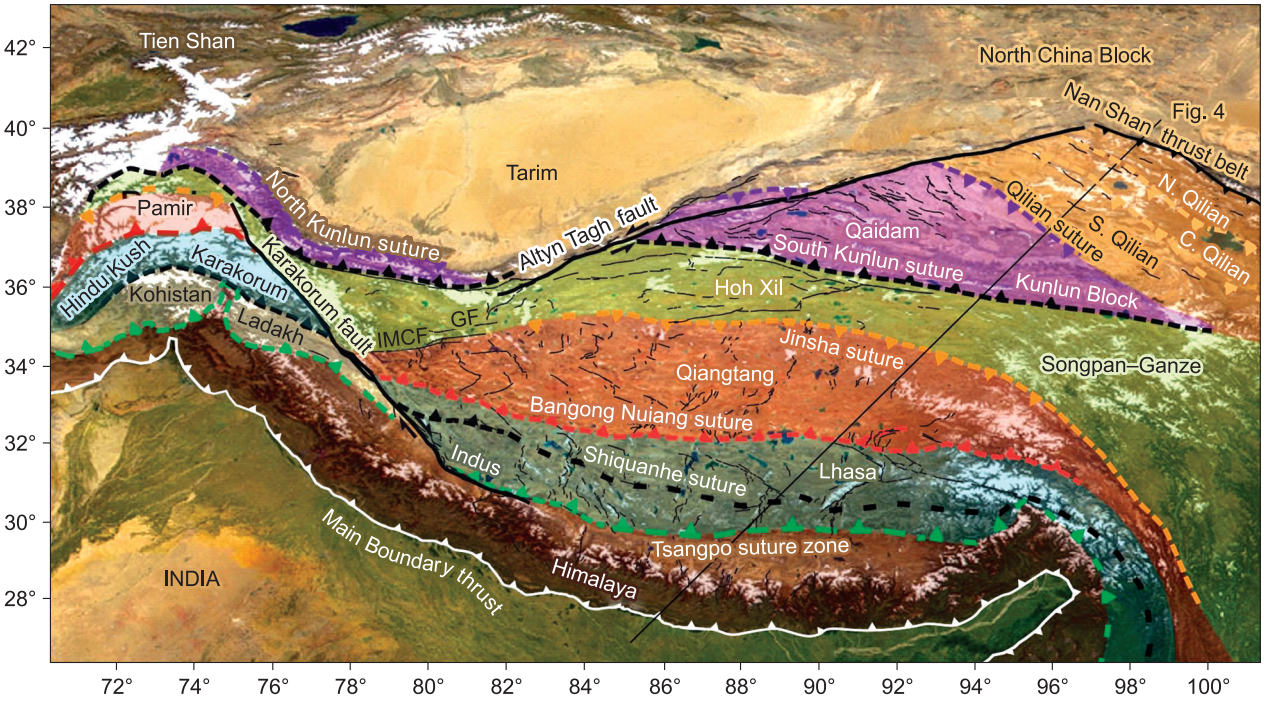

Fig. 3. Simplified geological map of the Tibetan Plateau showing the different accreted terrains separated by major suture zones (modified from (Guillot and Replumaz, 2013)).

The black line marks the emplacement of the cross section of Fig. 4.

Hoh Xil basin, Permian to Quaternary rocks are exposed along the Fenghuoshan Range and in the surrounding regions. The continental sedimentary rocks exposed within the Hoh Xil Basin are from Late Cretaceous to Miocene (Staisch et al., 2016 and references therein). The Late Cretaceous (Cenomanian) to early Eocene (Ypresian) Fenghuoshan Group is the first record of continental sedimentation and uplift above sea level (Staisch et al., 2014). The basin development and the deposition of the Fenghuoshan Group was likely caused by the loading of the foreland basin and erosion of the rising Tanggula fold and thrust belt (TFTB). No evidence of postdepositional deformation has been recognized in the Fenghuoshan Group, suggesting that the crustal shortening did not propagate into the Hoh Xil basin after ~51 Ma (Staisch et al., 2016).

South of the Jinsha Suture, the Qiangtang terrane forms the most central terrane of the Tibetan Plateau (Figs. 3, 4). Westwards, it extends to the Central Pamir region, where it could correlate with the North Karakorum terrane (Searle and Tirrul, 1991). The northern Qiangtang terrane hosts Early Cretaceous to mid-Eocene continental volcanosedimentary basins, separated from Carboniferous to Triassic sedimentary series by south-verging thrust systems. In the middle of the Qiangtang terrane, ultramafic and metamorphic rocks outcrop. The widest outcrop constitutes an anticline of more than 200 km long, in which a tectonic and metamorphic mélange is exhumed along faults detachments, and brought into contact with Carboniferous to Triassic overlying sedi-

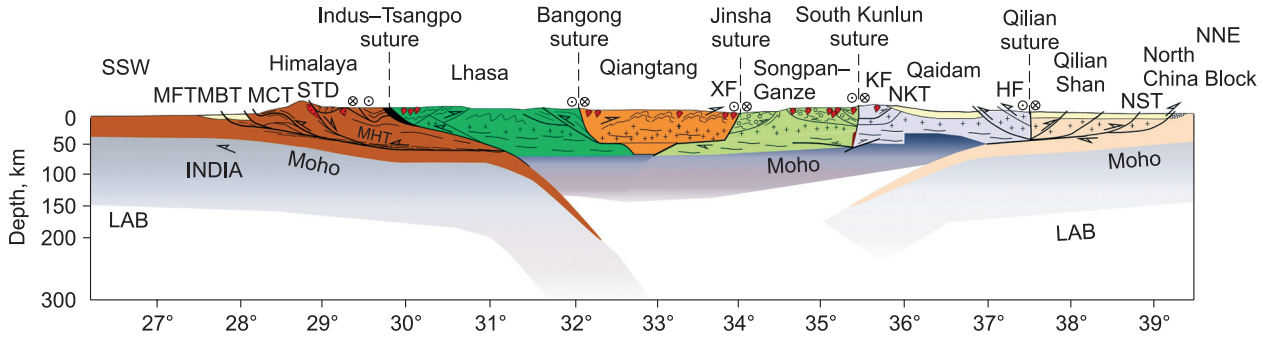

Fig. 4. Cross-section from Himalaya (SSW) to the North China Craton (NNE), along the line reported in Fig. 3 (modified from (Guillot and Replumaz, 2013)).

ments. This mélange locally preserves relicts of blueschist and eclogite-facies rocks of Middle Triassic age (Pullen et al., 2008; Zhang et al., 2018). This metamorphic belt was initially interpreted as an accretionary prism related to the southward subduction of the Songpan-Ganze terrane (Kapp et al., 2003; Pullen et al., 2008). Discovery of the oldest Tibetan ophiolites (between 501 and 437 Ma) along the Longmu Co-Shuanghu suture confirms that this belt corresponds to a remnant of the Longmu Co-Shuanghu Ocean separating the North and South Qiangtang terranes (Zhang et al., 2016).

Paleogene continental lacustrine basins are widely distributed across the Qiangtang terrane (e.g., (Ding et al., 2003)). They are bounded by north-dipping thrust faults (Kapp et al., 2005). This sedimentation indicates that west–central Tibet was above sea level since the mid-Cretaceous and experienced significant denudation prior to Paleogene. Early Cretaceous uplift is related to the south thrusting of the Qiantang terrane over the Lhasa terrane with 70 to 150 km of north–south displacement is estimated (Kapp et al., 2007).

The Bangong-Nujiang suture separates the Qiangtang terrane from the Lhasa terrane (Figs. 3, 4). It forms an intensely deformed accretionary complex composed of a dismembered ophiolitic sequences dated at 167–132 Ma (Li et al., 2017 and references therein). Arc magmatism occurs along the southwestern Qiangtang margin and is dated from 185 to 84 Ma (e.g., (Li et al., 2017)). It marks the closure of the Meso-Tethys ocean along a north-dipping subduction. Metamorphic rocks are rare along the suture of Bangong-Nujiang. Amdo granulitic gneisses provided ages of 190–180 Ma suggesting thickening of the crust at that time (Guynn et al., 2012). Kapp et al. (2005) described mid-Cretaceous nonmarine red beds and volcanic rocks lying unconformably on the Jurassic suture zone rocks along the Bangong suture. One hundred km south of the Bangong suture, the Shiquanhe-Gaize-Amdo north-dipping thrust, active during the Eocene–early Oligocene, is attributed to the northward underthrusting of the Lhasa terrane beneath the Qiangtang terrane (Kapp et al., 2005).

The two-thirds of the southern Lhasa Block are occupied by the Gangdese batholith (120–40 Ma). In the east and in the middle of the terrane, Ordovician sediments and Permian shallow marine carbonates and volcaniclastic deposits crop out. They are associated with ultramafic rocks and rare Permian eclogites (Yang et al., 2009). The assemblage represents an intrasuture zone within the Lhasa terrane (Yang et al., 2009; Zhu et al., 2011b) likely related to the opening and closure of back-arc basins along the northern margin of Gondwana (Zhu et al., 2011a). Triassic carbonate, turbidite and volcanoclastic deposits, rarely associated with magmatism, crop out in the southeastern part of the Lhasa terrane and have been related to the early subduction of the Neo-Tethys under Lhasa (Wang et al., 2016). Jurassic sediments made of alternating sandstone, clay, carbonate and volcanic rocks occupy instead the entire northern half of the Lhasa terrane. Their thickness increases northwards, until forming a sequence of 15 km thick flyschs along the Bangong suture (Marcoux et al., 1987; Kapp et al., 2003). The Cretaceous is marked by a major marine regression: whereas the Lower Cretaceous middle marine carbonates are widely spread through almost the entire Lhasa terrane, the Late Cretaceous marine sedimentation is restricted to deep flysch deposits at the north along the Bangong suture and south borders of the block, close to the Xigaze forearc basin (Yin and Harrison, 2000). The emersion is associated to an intense shortening along the Bangong suture. Syntectonic basins accommodate hundreds of kilometers of shortening between the Late Cretaceous and the early Cenozoic, In the Xigaze Basin, the Cenozoic sedimentation (up to the Oligocene) is characterized by fluvial facies (Dürr, 1996). In the rest of the terrane, Cenozoic continental sediments are rare, and the quasi-absence of deformation of the Paleocene–Eocene volcanic sequence of Linzinzong indicates that the southern upper crust of Lhasa did not experience significant shortening after the Cretaceous (Yin and Harrison, 2000)

The Lhasa terrane is separated from the Indian Plate by the Indus–Yarlung–Tsangpo suture (Figs. 3, 4). This suture, underlying the closure of the Tethys realm, is underlined by an intensely deformed radiolarite-rich sedimentary unit of Upper Jurassic–Middle Cretaceous and interpreted as an accretion prism. Several ophiolitic massifs, Early Cretaceous in age, are also present (Mahéo et al., 2004; Hébert et al., 2012; Buckman et al., 2018), with the exception of the Zedong-Luobusa to the east, which is dated of Middle Jurassic. These ophiolites are the remains of the Neo-Tethys Ocean, which closed along at least two north-dipping subduction zones: an intraoceanic subduction, at the origin of the Kohistan-Ladakh arc, and an Andean type ocean-continent subduction beneath Lhasa which gave rise to the Gangdese batholith and Linzizong volcanism. Associated magmatism has gone through two major phases, between 100 and 80 Ma then between 65 and 45 Ma, but started as early as the Upper Triassic (210 Ma) and continued until the Miocene (10 Ma) following the subduction-collision of the Indian continent (Zhu et al., 2017 and references therein). The Indus suture shows some metamorphic record in the blueschist-facies, linked to the Cretaceous functioning of the accretionary prism. These rocks have metamorphic ages between 100 and 80 Ma (Guillot et al., 2008 and references therein). The continental eclogites of Stak, Kaghan and Tso Morari in the NW Himalaya have ages between 46 and 55 Ma and record the onset of subduction of the Indian margin beneath the intraoceanic-arc, then beneath the south Asian margin (de Sigoyer et al., 2000; Guillot and Replumaz, 2013).

THE EVOLUTION OF THE PALEOALTITUDE OF THE TIBETAN PLATEAU

The timing of growth of the Tibetan Plateau is intimately related to its uplift. The stepwise subduction model of Tapponnier et al. (2001) imposes that the uplift of the Tibetan Plateau propagates northward since 50 Ma. In contrast, the lithospheric root delamination model of Molnar (1988) constraints a rapid and general uplift of the plateau at about 10 Ma. An increasing amount of data suggests that a large part of the Tibet was already high before the India–Asia collision. Two types of indicators constrain the elevation of the Tibetan Plateau. On one hand, qualitative indicators deduce an elevation gain accordingly to major tectonic changes (compression extension transition), magmatic (appearance of shoshonitic and/or adakitic magmatism), sedimentary (late marine sedimentation, transition to internal continental drainage), metamorphic (acceleration of cooling, or on the contrary slow and continuous cooling which indicates an absence of thickening for a certain period) or topography (incision rivers, distribution of fauna). On the other hand, quantitative indicators of paleoaltimetry of sedimentary basins have been developed in recent decades. They include:

– paleobotany: a comparison with the current flora, the temperature of the air or the concentration of CO_2 (via the stomatal frequency on the leaves) are estimated;

– palynology: paleoelevations are calculated according to the mean annual temperature (MAT) estimated using specific pollen taxa. Microthermic trees inhabiting high elevation/high latitude zones, such as Abiesand Picea, represent the best indicators of elevated topography in the fossil pollen floras (Fauquette et al., 1999, 2015);

– stable isotopes of oxygen in carbonates, possibly associated with stable isotope measurements of carbon in the "clumped isotope" (method of (Ghosh et al., 2006)) are compared to the present-day values in Himalaya;

– the stable isotope of hydrogen (deuterium) in the organic fraction of rocks (vegetable lipids *n*-alkanes).

These different paleoaltimetric methods can give altitudes differing from nearly 2500 m, the isotopic methods generally providing the highest altitudes. Furthermore, isotopic paleoaltimeters suffer of many assumptions such as the effects of diagenesis and evaporation, the paleotemperatures, the distance to ocean basins and the type of atmospheric circulation at the time of the deposit. The monsoon system for example, increases the isotopic fractionation of oxygen and hydrogen. Paleoaltitudes deduced from the same isotopic ratio $^{18}O/^{16}O$ can thus vary from simple to double according to the initial hypotheses (Deng and Ding, 2015).

Furthermore, an increasing number of indirect evidence (tectonic, thermochronology, metamorphism) indicate that the central part of the Tibet, from south Qiangtang to the Songpan Ganze was above the sea level since the Eocene and potentially since the Mesozoic (Fig. 5) due to the successive collision among the different terranes (Kirby et al., 2002; Dai et al., 2012; Jolivet, 2017). In the Longmen Shan (eastern Tibetan Plateau) petrochronological data demonstrate that the upper crust was already 30–35 km thick at the Late Triassic (Airaghi et al., 2017a, 2018a,b; Zhang et al., 2018) and was reactivated by mid-Cretaceous time (Airaghi et al., 2017b, 2018a; Xue et al., 2017). By considering a 20 km thick lower crust, it is thus possible to calculate a minimum altitude of 2000–2500 m at the Cretaceous times. This is consistent with clumped isotope temperatures of Li et al. (2019) and Rohrmann et al. (2018) showing that before 50 Ma, the Nangqian basin in Central Tibet was at an altitude of 2700 m (+600/–400 m) above sea level. The hypsometric mean elevation of surrounding mountains was 3000 ± 1100 km above sea level. Along the Bangong suture, Kapp et al. (2007) estimated more than 100 km of shortening during mid-Cretaceous time, which also indicate continental crustal thickening and consequently relatively high elevation. The southern active margin of Lhasa was also relatively high (Andean type margin) during the Late Cretaceous (Kapp et al., 2005; Wang et al., 2014). Whole-rock La/Yb ratios of intermediate intrusive rocks from the Gangdese arc indicates that the Southern Lhasa crust was of normal thickness prior to approximately 70 Ma (~37 km), the crust reached 58–50 ±10 km of thickness at 55–45 Ma, extending over 400 km along the arc strike by magmatic underplating and 68 ± 12 km at c. 20–10 Ma, as a consequence of underthrusting of India and of the associated thrust faulting (Zhu et al., 2017). The same authors also suppose that the Gangdese attained an elevation of > 4000 m at approximately 55–45 Ma. In northeastern Tibet, low-T thermochronology data indicate the presence of intact surfaces since the beginning of the Mesozoic.

This relatively high pre-collision elevation in Tibet is associated with evidence of crustal deformation from the Gangdese in the south to the Songpan-Ganze in the North, related to crustal shortening from c. 60–80 to 40 Ma (Staitsch et al., 2016 and references therein; Horton et al., 2002) (Fig. 6). Between the Oligocene–Miocene and the Pliocene (23–8 Ma), this Tibetan protoplateau spread north and south to the Kunlun Mountain and Himalaya while in the central Tibet the deformation ceased (Fig. 6). The flat-lying ~27 Ma basalts in the Hoh Xil Basin (Staisch et al., 2014), the 28 Ma old undeformed volcanic rocks in the Yulin Shan (Xu et al., 2013) as well as the rarity of evidence for postcollisional deformation in the Lhasa and Qiangtang terranes (Burg et al., 1984; Murphy et al., 1997; Ding et al., 2007; Kapp et al., 2007; Wang et al., 2008) suggest that upper crustal shortening of the Tibetan Plateau was largely completed by the early Miocene (~20 Ma). The

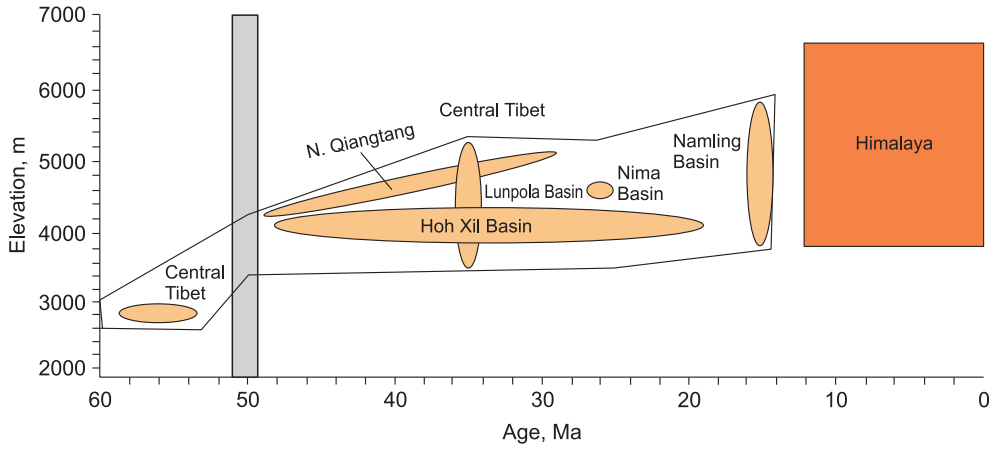

Fig. 5. Paleoaltimetry results in Central Tibet (modified from (Wang et al., 2014)).

continued convergence between India and Eurasia must have therefore been accommodated outboard of the Tibetan Plateau, in the Himalaya, in the Qilian Shan, and in the northeastern plateau margin (Staitsch et al., 2016). In fact, the maximum height of mountains was reached in the Himalaya after 25 Ma, in Tien Shan after 20 Ma, in Dzhungaria after 10 Ma, in Altai after 5 Ma, and in Cisbaikalia (Sobel et al., 2006; Glorie et al., 2010, 2011, 2012; Delvaux et al., 2013; Jolivet, 2017).

THE CENOZOIC MAGMATIC EVOLUTION OF THE TIBETAN PLATEAU

The pre-Himalayan history of the Proto-Tibet recorded a long-lived magmatic evolution related to the closure of oceanic domains and subsequent accretion of continental terranes giving birth to a Mesozoic Andean-type magmatism. In this paragraph, we will focus on the Cenozoic ("postcollisional") magmatism of the Tibetan Plateau, as it is the most likely to provide information on the composition of the source mantle at the time of the construction of the Tibetan plateau.

At a first glance, the migration of postcollisional magmatism across the Tibetan Plateau during the Cenozoic seems to reflect the growth of the Tibetan Plateau (Fig. 6). Different causes for magmatism have been proposed: for some authors, it is due to asthenospheric flow from the center to the plateau margins, assuming the asthenosphere as the necessary source of heat for the melting of the lithospheric mantle (Mo et al., 2006). For other authors, each phase of postcollisional magmatism testifies the reactivation of a suture (Ding et al., 2007; Guillot and Replumaz, 2013).

Postcollisional magmatism exhibits atypical chemical compositions and a complex distribution through time. The lavas of Linzizong (60–45 Ma), a part of the batholith of Gangdese in south Lhasa (Fig. 7), belong to a sodic calk-alkaline series, and are of basaltic to rhyolitic composition. Several types of mantle sources have been identified as contributing to the source of these lavas: the oceanic lithospheric mantle (DUPAL) of the Neo-Tethys, the continental lithospheric mantles of India and Lhasa, and the Lhasa crust, including the root of

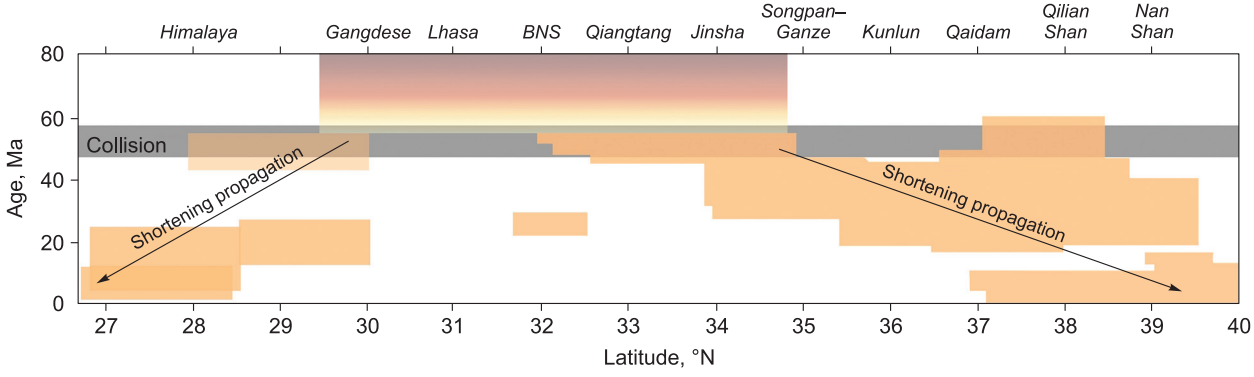

Fig. 6. Age of crustal shortening as a function of the latitude (from Himalaya to Tibet).

The southern and central Tibet were already involved into the deformation and uplifted prior to 50 Ma. After this period, deformation propagated northwards and southwards (modified after (Staitsch et al., 2016)).

the batholith of Gangdese, partially re-melted during volcanism (Wang et al., 2016). A strong magmatic flare up is recorded at 52–51 Ma. It is interpreted as break-off of the subduction Indian Plate (Zhu et al., 2015) although tectonic reconstruction constrains the age of the Indian break-off at 45 Ma (Replumaz et al., 2010). The shift of 6 Ma between magmatic and tectonic reconstruction will be due to the time difference between the magmatism that can occur from the initiation of the slab break-off while the complete break of the Indian slab image by tomography can occur later.

Along the northern edge of Qiangtang, small volumes of igneous material are emitted within intramontane basins between 50 and 30 Ma, forming a ca. 2000 km long volcanic belt (Fig. 7). These mafic to felsic rocks are characterized by enrichment in potassium and belong to the potassium-rich calk-alkaline series (Fig. 8). The high potassium contents are associated with a strong relative enrichment in light rare earth elements and in LILE (large radius elements ionic, easily mobilized by fluids), a fractionation of heavy rare earth elements, and a poor content in HFSE (elements with high loads, hardly mobilized by fluids) generating an arc signature (Ding et al., 2007; Xu et al., 2017; Goussin, 2019). In central Qiangtang, some of these potassic rocks have an adakitic signature with high levels of Sr and low Y (Wang et al., 2008). In the southern Qiangtang a discontinuous calk-alkaline magmatism is observed between 60 and 28 Ma, comparable to the one documented in the northern Qiangtang, but enriched in sodium rather than in potassium (Ding et al., 2003, 2007).

Between 26 and 10 Ma, the magmatic activity of the Tibetan Plateau is located in the southern Lhasa Block, along a 1500 km long band (Fig. 7). This magmatism is associated with extensive northsouth oriented rifts. The compositions of the Lhasa igneous rocks can be divided into two groups. The ultrapotassic calk-alkaline rocks, mafic to intermediate, presenting trace elements enrichment similar to the ultrapotassic lavas of Qiangtang are found in the western part of the block (<87° E). They are interpreted as related to the second break-off of the Indian slab (Mahéo et al., 2002). The second group of igneous rocks is intermediate to felsic, calk-alkaline and potassium-rich and exhibit an adakitic signature symptomatic of the melting of the lower crust (Gao et al., 2007).

From the Miocene to the present day (the last recorded eruption on the Tibetan Plateau took place in 1951), a resumption of magmatic activity took place in the western Songpan-Ganze Block (Hoh Xil Basin). Two types of rocks are emitted: calk-alkaline intermediate rocks in the Hoh Xil basin, slightly depleted in potassium than their Eocene analogues and peraluminous leucogranites (so-called S-type: fusion products of a sedimentary source) in the Ulugh Muztagh region.

The northeastern and southeastern edges of the Tibetan Plateau (Fig. 7) are affected by potassic lavas with postcollisional ultrapotassic compositions called “kamafugites”. They are accompanied by carbonatitic lavas, composed by 60% of calcite (Yang and Woolley, 2006). The two main carbonatitic provinces bordering

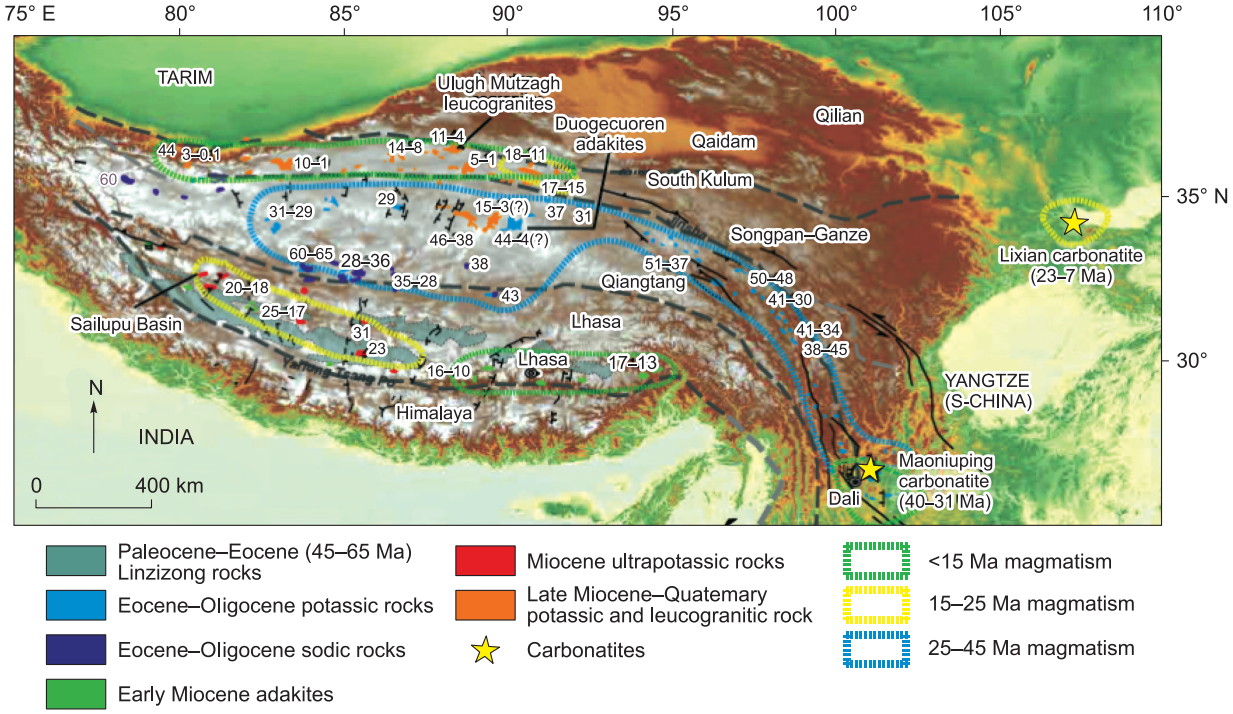

Fig. 7. Map of the potassic to ultrapotassic Cenozoic magmatism of the Tibetan Plateau (modified from (Wang et al., 2014)).

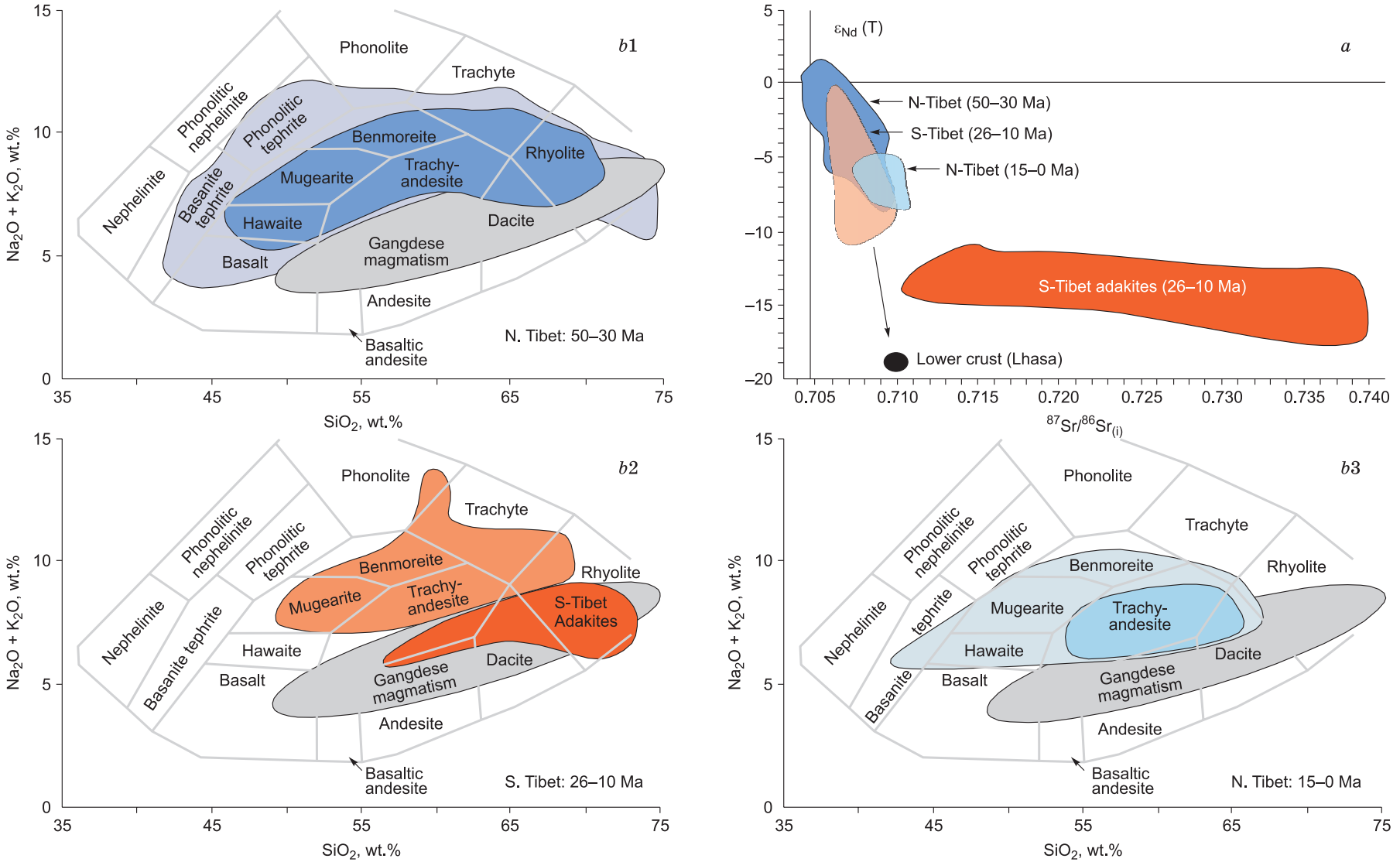

Fig. 8. Composition of the Cenozoic igneous rocks of the Tibetan Plateau. *a*, **Nd–Sr isotope compositions at T = rock ages;** *b*1, *b*2, *b*3, **Alkaline and silica contents from the different magmatic provinces. The gray field corresponds to the Gangdese calk-alkaline magmatism. Figures from (Chung et al., 2005).**

the Tibetan Plateau are that of Lixian in the western belt of Qiling (23–7 Ma) (Xu et al., 2014), and that of Maoniuping in Sichuan (40–31 Ma) (Xu et al., 2003). These occurrences of carbonatites in a compressive setting are rare as this kind of rocks is more frequently encountered in rifting conditions and related to deep plume activity (e.g., Ol Doinyo Lengai in Tanzania, Kaiserstuhl in Germany). Tibetan carbonatites are similar to the carbonatites found in the Pleistocene magmatic province of the Apennines (Italy), interpreted as due to a strong metasomatism of the lithospheric mantle wedge by the CO_2 released from subducted sediments, or to later crustal interactions with the host carbonates (Peccerillo, 2004).

Chemical, experimental studies and modelling of the behavior of trace elements indicate that magmas come from a low degree of partial melting of a metasomatized lithospheric mantle phlogopite and/or amphibole, in the stability field of garnet (>100 km) (Turner et al., 1996; Miller et al., 1999; Ding et al., 2003; Guo et al., 2006). The contrast between the homogeneity of rare earth elements spectra and the high variability of isotopic signatures (Nd–Sr, Hf) between the different magmatic sequences suggests however, that their respective sources had a specific metasomatic history, at different times, that involves different metasomatic agents in terms of nature and ages. The compositions of rocks of the Lhasa Block highly-enriched in $^{86}Sr/^{87}Sr$ are explained for example by a hybridization between mantle and crustal melt liquids (Wang et al., 2016; Stepanov et al., 2017). The special case of sodium-rich magmas of South Qiangtang has been interpreted instead as reflecting interactions with an igneous crust rather than metasediments (Ding et al., 2007). The "adakitic" signature observed in some Tibetan rocks generally reflects the implication of a deep melting of oceanic crust in the genesis of magmas. Two sources have been supposed for Tibetan adakites: the lower mafic crust, in the context of a thickened crust (Chung et al., 2005); or the metasomatized mantle (Gao et al., 2007).

Finally, the carbonatite and kamafugite associations at the borders of the Tibetan Plateau have long been seen as products of interaction between the asthenospheric and the lithospheric mantle (Lai et al., 2014 and references therein). In fact, carbonatites in association with ultrapotassic kamafugites are usually interpreted as the surface expression of deep mantle plume (Maruyama, 1994; Ernst and Buchan, 2002; Dobretsov et al., 2008). However recent studies have re-evaluated Sichuan carbonatites as melting products from a lithospheric mantle intensely metasomatized by marine subducted sediments rather than originated from a mantle plume (Xu et al., 2003; Lai et al., 2014).

At present, the mantle xenoliths and xenocrysts sampled on the Tibetan Plateau are rare and come from two sites: the Miocene volcanic rock pool (26–8 Ma) of Sailipu, in the Lhasa Block (Liu et al., 2011; Cheng and Guo, 2017) and from the Eocene Nangqian igneous rocks in the Qiangtang Block (Goussin et al., 2017). At Sailipu, Cheng and Guo (2017) described websterites and harzburgites containing 3 to 5 vol.% of phlogopite. The harzburgites show a high content potassium (0.1–0.5 wt.%) and iron (10–11 wt.%). The occurrence of phlogopite confirms the metasomatism of the Tibetan lithospheric mantle identified in the composition of the associated igneous rocks. Their equilibration temperatures (1069–1248 °C) indicate a hot mantle geotherm during the Miocene under the Lhasa Block (Liu et al., 2011). In the Nangqian area, only xenocrysts of large (mm) zoned phlogopites enriched in MgO are found inside an ultra-potassic syenite. Interestingly, massive potassic lavas also contain aggregates with coarse-grained cumulate textures consisting of finely zoned clinopyroxene crystals, rare resorbed magnesian phlogopite and calcite that fills the grain boundaries and cracks, often in association with apatite, ilmenite and rarely barite. Stable isotopes demonstrate that the calcite derived from the mantle (Goussin et al., 2017). This confirms that the Tibetan mantle was metasomatized by hydrous and carbon-rich fluids.

SEISMIC TOMOGRAPHY OF THE TIBETAN MANTLE

Seismic tomography is an important source of information on the structure, composition and/or thermal state of the Tibetan mantle. P-wave tomography highlights several areas of high velocities, located at different depths. These anomalies are interpreted as lithospheric slabs colder than the surrounding mantle. Some are related to active subductions. This is the case for the Indian slab that dips shallow beneath South Tibet up to the Bangong suture, and then dives vertically (Koulakov and Sobolev, 2006). Other deeper anomalies could correspond to fragments detached during previous subductions: an anomaly at 1000 km depth is interpreted as the Neo-Tethyan ocean slab, another at the transition zone as a detached Indian continental lithospheric slab, and a last, rather diffuse (Fig. 9), as an "Asian" lithospheric slab (Van der Voo, 1999; Guillot and Replumaz, 2013).

P-wave tomography also reveals a low-velocity anomaly below the Qiangtang and Songpan-Ganze terranes (Liang and Song, 2006). This anomaly has often been interpreted as the replacement of the root of the lithosphere by asthenosphere (Molnar, 1988; Tunini et al., 2016); but it could also represent a metasomatized lithosphere (Zhang et al., 2014; Tunini et al., 2016). The hypothesis of lithospheric delamination is challenged by other types of seismological studies, imaging the lithosphere-asthenosphere boundary (LAB). Receiver function profiles suggest that the LAB is between 180 and 200 km depth below the Tibetan Plateau, only 50 km

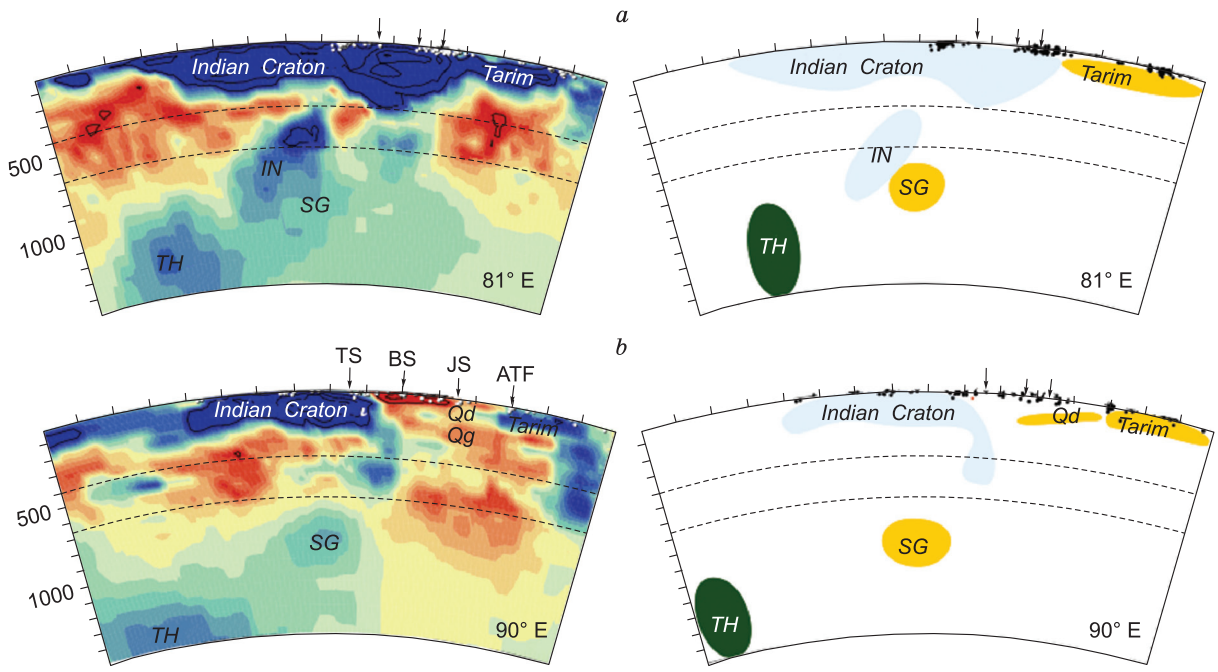

Fig. 9. *a*, P-wave tomography of the Tibetan mantle along two cross sections at two different longitudes.

At 81° E of latitude, we distinguish the deep rapid anomalies corresponding to the slabs detached from the Neo-Tethys (TH), the Indian continental margin (IN), and a diffuse Asian lithospheric slab interpreted as the detached Songpan–Ganze Asian slab (SG). *b*, At latitude 90° E, we distinguish the current Indian slab dipping vertically beneath the suture of Bangong, as well as a slow anomaly often interpreted as an asthenospheric rising under a thinned Tibetan lithosphere. TS, Tethyan Suture; BS, Bangong suture; JS, Jinsha suture; ATF, Altyn Tagh fault; Qd, Qaidam. Figures modified after (Replumaz et al., 2014).

shallower than the Indian LAB, that does not show any trace of large-scale delamination (Zhao et al., 2010, 2011). On the contrary, the easternmost profile shows the existence of a thick Asian lithosphere subducting southward, creating an Asian LAB symmetrical to the Indian LAB (Kind et al., 2002; Zhao et al., 2010) (Fig. 10).

Furthermore, since the S-waves velocities (V_s) are more sensitive to temperature variation than P-waves, the LAB can be interpreted in terms of change of thermal transfer, from conductive to convective. This results in a large increase of the thermal gradient. Thus, regional variations of V_s can be related to variations in lithospheric thickness (Priestley and McKenzie, 2006, 2013). It has been proposed that V_S profiles under Tibet are very similar to that of cratons characterized by a lithosphere up to 300 km thick (Priestley and McKenzie, 2013, fig. 1.31; Priestley et al., 2006). However, their poor lateral resolution does not rule out small-scale delamination

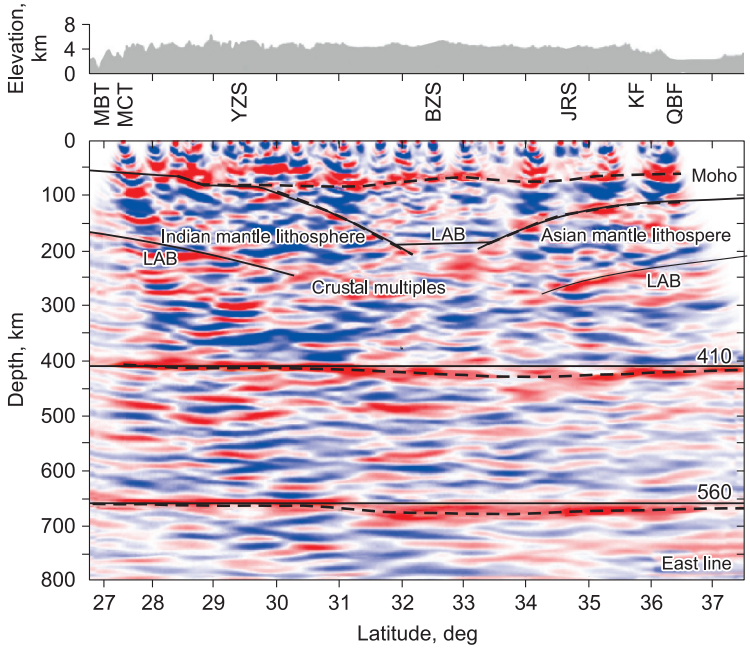

Fig. 10. Receiver functions profile across the Tibetan Plateau showing the existence of a south-dipping Asian slab without evidence of delamination of the Tibetan lithosphere (from (Zhao et al., 2010)).

MBT, Main Boundary Thrust; MCT, Main Central Thrust; YZS, Yarlung Suture Zone, BNS, Bangong suture zone; JRS, Jinsha River suture; KF, Kunlun fault; QBF, Qilian Shan North Margin Fault.

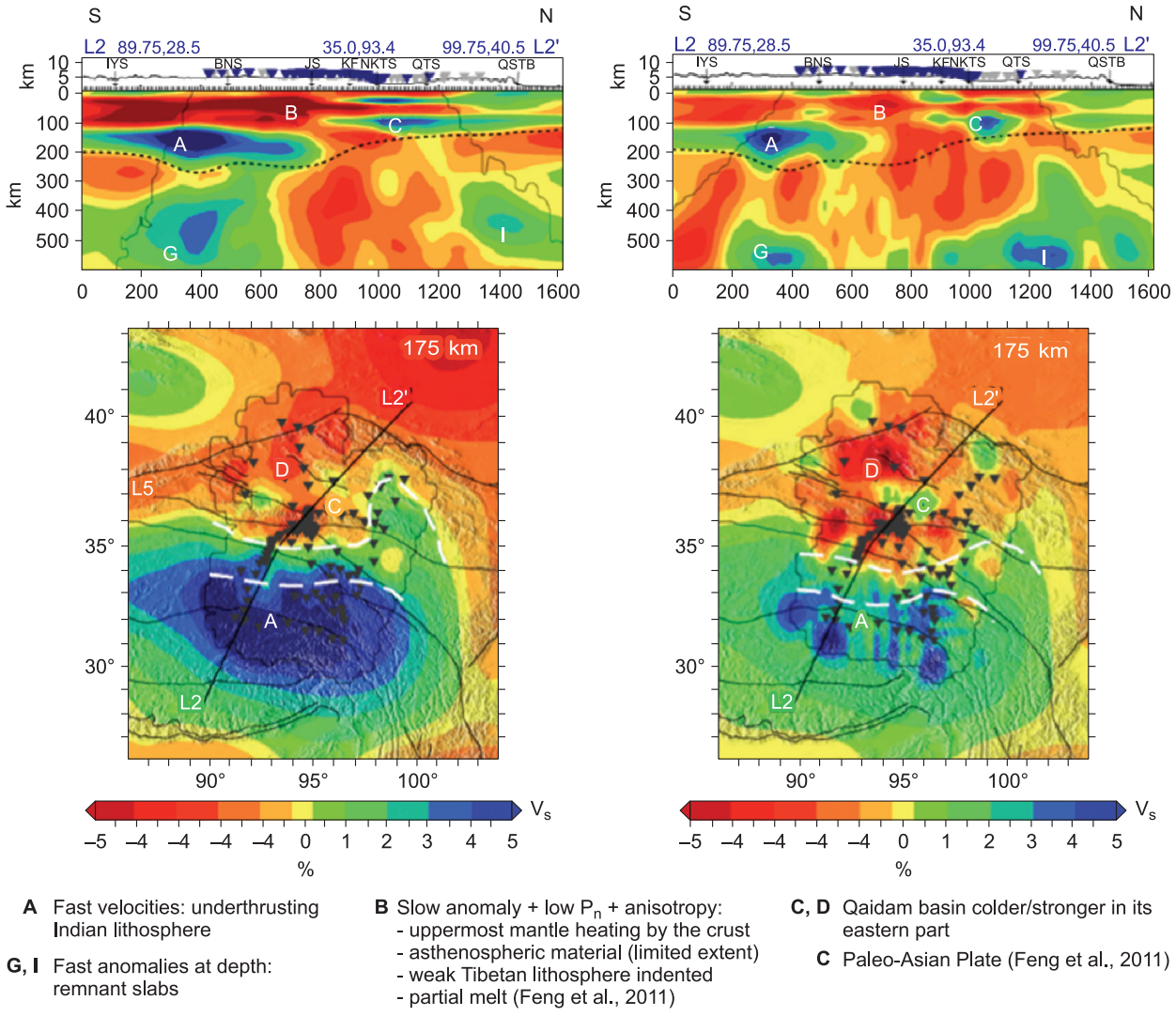

Fig. 11. Seismic Tomography of the Northeast Tibetan Plateau resulting from the joined inversion of surface and volume waves.

Contrasts of V_p (in%). The LAB is indicated with a dashed lines. IYS, Indus Yarlung suture, BNS, Bangong suture; JS, Jinsha suture; NKTS, North Kunlun Thrust system; QTS, Qiangtang Thrust System; QSTB, Qilian Shan Thrust belt (modified from (Nunn et al., 2014)).

(Priestley et al., 2006). The poor lateral resolution of S- and P-wave tomography has been greatly improved in jointly reversing the surface wave data (which provides a crustal correction) and shear volume waves. This type of tomography confirms the existence of a thick lithospheric root beneath the entire Tibetan Plateau formed by a "stacking"of noncratonic lithospheres (110 km thick) (Feng et al., 2011). In high-resolution tomographic images, a slow anomaly zone (B) is visible under the northwest Qiangtang and west Songpan-Ganze, between the middle crust and 120 km depth (Fig. 11) (Nunn et al., 2014).

This anomaly, strictly limited to the northwest of the Tibetan Plateau seems to affect only the first ten kilometers of the lithospheric mantle and could just be the consequence of a warming by overthickened radiogenic overlying crust (Nunn et al., 2014) leading to the local partial melting of the upper mantle (Feng et al., 2011). The presence of asthenospheric material cannot however be discarded (Fig. 12).

Goussin et al. (2017) show that the addition of phlogopite and carbonate (magnesite) to the Tibetan lithospheric mantle along a normal geotherm reproduces the present-day V_p anomaly (Guillot and Replumaz, 2013), shear wave velocity profile (Vozar et al., 2014), and low mantle density inferred from the topography and gravity data of the Tibetan Plateau (Tunini et al., 2016). A normal thickness of a metasomatized and buoyant lithospheric mantle in Central Tibet can thus explain the geophysical observations without recourse to a thermal anomaly associated with a thinned lithosphere and asthenosphere upwelling. It would also be consistent with

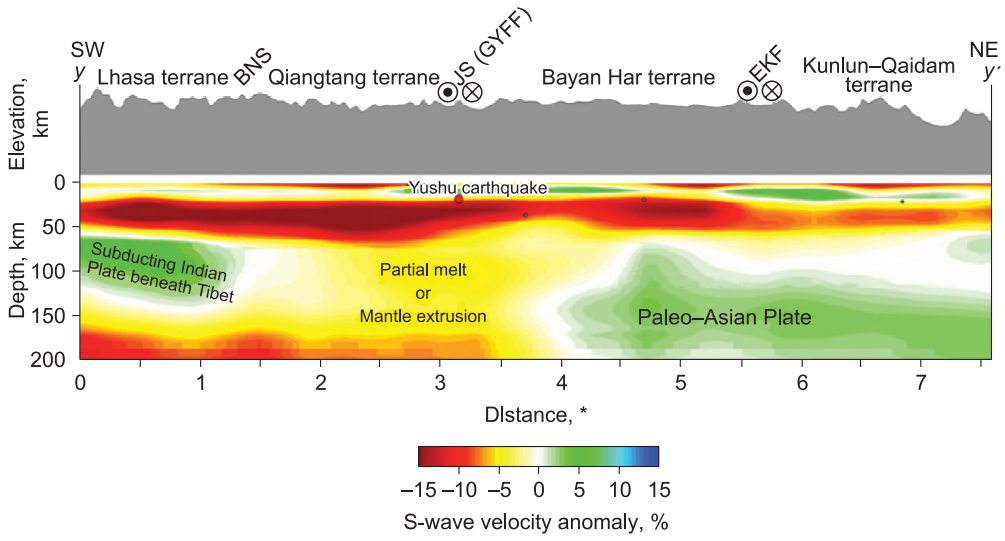

Fig. 12. S-wave velocity transects crossing the Ganze–Yushu–Fenghuoshan Fault. Black circles: historic earthquakes, black dashed line:

Moho discontinuity, BNS, Bangong–Nujiang suture; JS, Jinsha suture; EKF, East Kunlun fault; GYFF, Ganze–Yushu–Fenghuoshan fault. The low-velocity S-waves anomaly beneath Central Tibet is either interpret as velocity as occurrence of melt at the Moho level or mantle upwelling (from (Feng et al., 2011)).

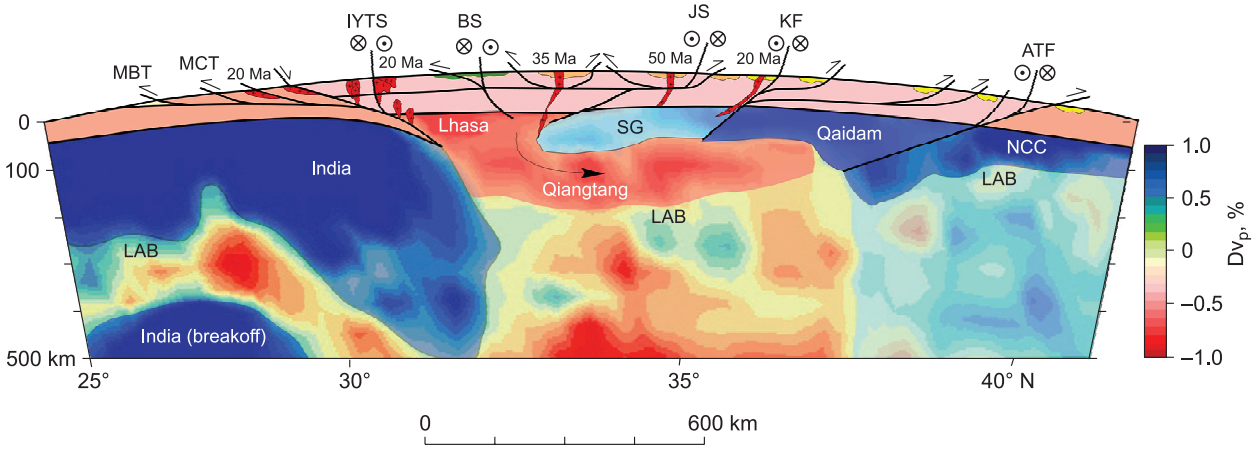

Fig. 13. Reinterpretation of the low V_p anomaly beneath Tibet (Section D of (Replumaz et al., 2013)) in term of metasomatized lithosphere rather than in term of asthenospheric upwelling.

In this interpretation, the moderate anomalies beneath Jinsha (SG) and the Altyn Tagh fault (NCC) corresponds to intracontinental low dipping subduction slab. The Qiangtang metasomatized lithosphere squeezed between the Indian slab and the Songpan–Ganze slab is push downward. The location of the LAB (Lithosphere Asthenosphere Boundary) at 200 km depth is similar to that in Zhao et al. (2010) and Nunn et al. (2014). The age of the Ultra-K magmatism is mentioned atop. MBT, Main Boundary Thrust; MCT, Main Central Thrust; IYTS, Indus Yarlung Thrust system; BS, Bangong suture; JS, Jinsha suture; KF, Kunlun Fault; ATF, Altyn Tagh fault; NCC, North China Craton.

the scarce measurements of a relatively low heat flow in Central Tibet (45 mW/m^2; (Vozar et al., 2014)). Goussin (2019) also show that the subcontinental mantle of Central Tibet in Eocene times would have weakened by one order of magnitude by the presence of phlogopite and carbonates.

The present-day position of the low-velocity P-waves anomaly beneath Central Tibet would correspond to the Lhasa and Qiangtang fossilized mantle wedges, squeezed and indented by the rigid Indian lithosphere to the south and the Songpan-Ganze lithosphere to the North (Fig. 13).

DISCUSSION

In the last decade, structural and paleoaltimetric studies have revealed that the southern margin of Eurasia, formed by the Lhasa terrane and the southern part of the Qiangtang Block, was already deformed before the onset of the India–Asia collision, due to a long lasting pre-Cenozoic history of continental accretions. A "Proto-Tibetan Plateau" had covered nearly 50% of the present-day surface of the plateau at the end of the Cretaceous (Kapp et al., 2007; Wang et al., 2008, 2014; Staisch et al., 2014). Considering that the Songpan-Ganze terrane was also already thickened at the Triassic and the Cretaceous (e.g., (Airaghi et al., 2017b, 2018a,b; Zhang et al., 2018)), the Proto-Tibetan Plateau was likely to represent two-thirds of the present-day Tibetan Plateau. Although it is difficult to estimate the paleoaltitude of this protoplateau, by assuming that the Moho depth was at ~50 ± 5 km as indicated by metamorphic and magmatic records, a paleoaltitude of 2500–3000 m can be expected before the India–Asia collision. Altitude values have locally reached >4000–4500 m, as in South Lhasa or along the Jinsha suture zone (Staish et al., 2016; Zhu et al., 2017). The shape and size of the Proto-Tibetan Plateau was therefore probably similar to the present-day Rocky Mountains or the Andes (Fig. 1), maintained by continuous subduction/accretion all along the Mesozoic.

Some authors supposed that the Proto-Tibetan Plateau underwent very limited deformation following the onset of the India–Asia collision (DeCelles et al., 2007; Kapp et al., 2003, 2005, 2007). However, 40% of horizontal shortening are required north of the Indus suture zone during the India-Asia collision in order to accommodate the ~1000 km of Cenozoic convergence on the Asian side that were estimated from paleomagnetic data and tectonic reconstructions (Dupont-Nivet et al., 2010; Guillot and Replumaz, 2013). This postcollisional deformation may have initiated in the central part of the present-day plateau (Fig. 6), in two fold-and thrust systems bordering the Jinsha suture zone. The Fenghuo Shan fold-and-thrust belt was shortened by 24% from 45 to 27 Ma (Staisch et al., 2016), and the Yushu-Nangqian fold-and-thrust belt was shortened by 40%, mainly from between ca 60 Ma to 35 Ma, with some resumption in the Neogene (Spurlin et al., 2005). These two belts may thus have accounted for 100 to 200 km of postcollisional shortening (Spurlin et al., 2005; Staisch et al., 2016). How this shortening was accommodated at depth remains however controversial.

Only homogeneous thickening of the whole lithosphere (Fig. 14) can be excluded on the basis of isostatic considerations: whatever the initial thickness conditions, the counterbalance between the buoyant thick crust and the less buoyant lithospheric mantle buffers the final elevations around 4000 m (Jiménez-Munt and Platt, 2006; Staisch et al., 2016). Moreover, as discussed above, P-wave tomography images the local preservation of continental slabs beneath Tibet (Figs. 9, 10, 13) rather than a thick and cold lithospheric root (Fig. 15).

In order to achieve the present-day mean elevations of 4500–5000 m, and the present-day crustal thickness of 70 km (Mechie et al., 2011), the alternative at the homogenous lithospheric thickening is the intracontinental subduction with underthrusting of the lower crust below the proto-Tibetan Moho (Tapponnier et al., 2001; DeCelles et al., 2002; Guillot and Replumaz, 2013; Maierová et al., 2016; Replumaz et al., 2016). The intracontinental subduction hypothesis in central Tibet is supported by the syncontractional emplacement of the northern Qiangtang Eocene–Oligocene postcollisional magmatism (Spurlin et al., 2005), forming an arcuate belt along the Mesozoic Jinsha suture zone. In fact, Bajolet et al. (2013) show by analog modelling that if the viscosity of the trench is low (<35 Pa·s), the subduction interface is highly lubricated. A more efficient lubrication of the trench allows more continent to subduct. The slab pull increases continuously, and when it approaches a positive value, the trend reverses and the curvature amplified forming an orocline convex opposite to the subduction polarity. Moreover, the magmatism has an arc-like geochemical signature and was likely derived from a metasomatized mantle source (Roger et al., 2000, Ding et al., 2003, 2007; Guo et al., 2006; Wang et al., 2008;

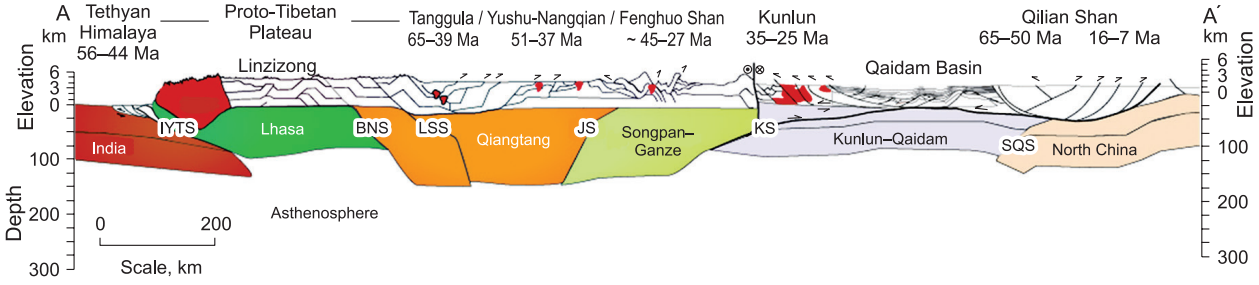

Fig. 14. Schematic cross-section across Tibet supposing a homogeneous thickening of 40% of the whole Qiangtang and Songpan–Ganze lithospheres (from (Goussin, 2019)).

The age of the Ultra-K magmatism is mentioned above IYTS, Indus Yarlung Thrust system; BNS, Bangong suture; LSS, Longmucuo–Shuanghu suture; JS, Jinsha suture; KS, Kunlun suture, SQS, South Qilian suture.

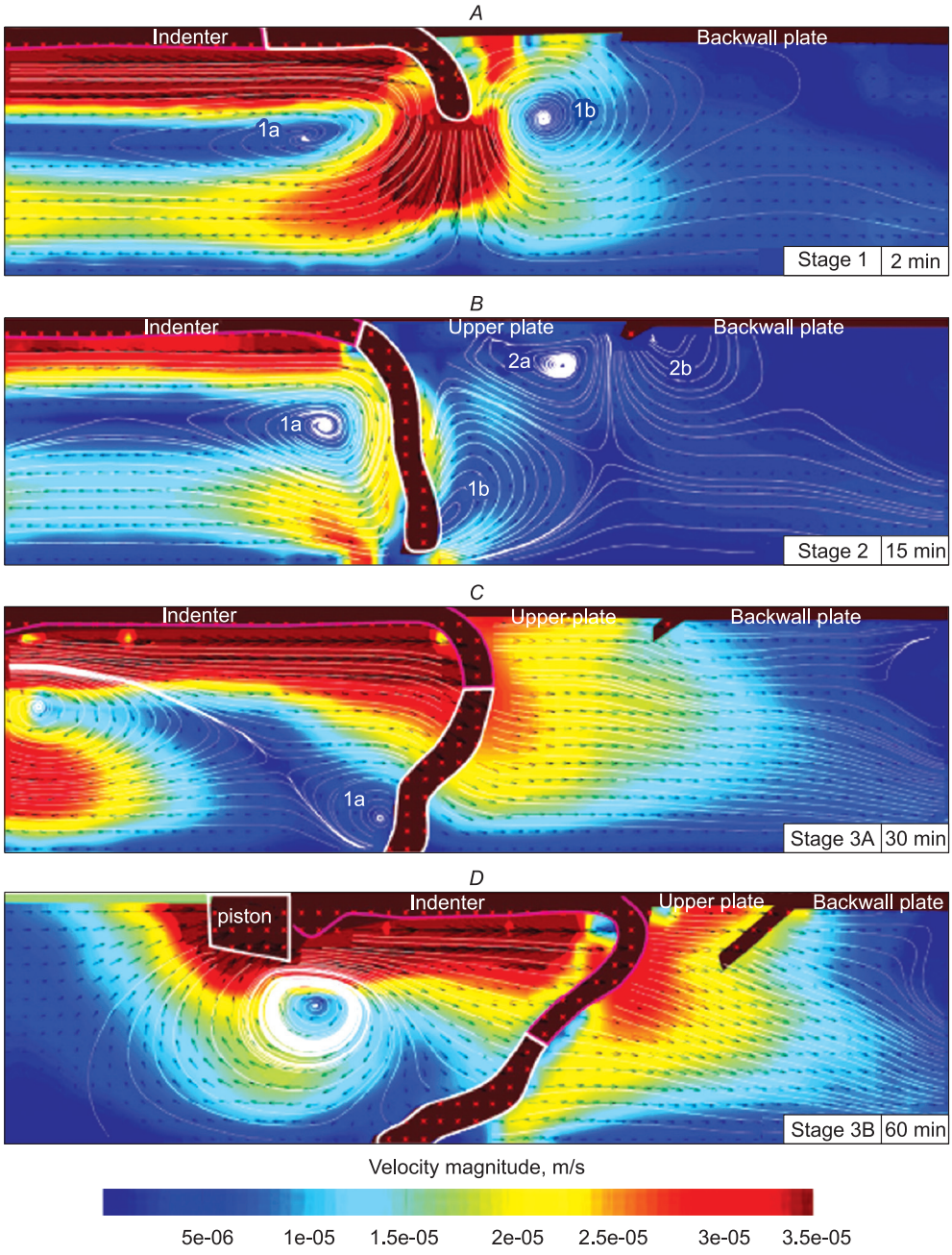

Fig. 15. Velocity magnitude recorded in glucose syrup modelling showing convective cells development below and front of the lower plate (1a and 1b) and below the upper plate (2a and 2b).

The development of convective cells 2a and 2b at the stage 2 initiated subduction collision processes in the upper plate that could be an equivalent of the Eocene continental subduction of the Songpan–Ganze slab along the Jinsha suture (Pitard et al., 2018).

Goussin, 2019). It has indeed been often attributed to the continental subduction of the Songpan-Ganze lithosphere beneath the Qiangtang terrane (Roger et al., 2000; Ding et al., 2003, 2007; Guo et al., 2006; Wang et al., 2008).

Accordingly to analog modelling, Replumaz et al. (2016) and Pitard et al. (2018) supposed that at the lithospheric scale, the horizontal tectonic force is higher than the resisting forces (buoyancy of the upper plate, bending of the slab, lithosphere/lithosphere interface resistances). As soon as the Indian continental slab entered the mantle, it changes the mantle circulation in particular below the upper plate. Assuming a lower viscosity for the upper plate than for the lower plate, such differential viscosity generates a smaller convective cell below the upper plate, favoring the initiation of continental subduction within the upper plate (Fig. 15).

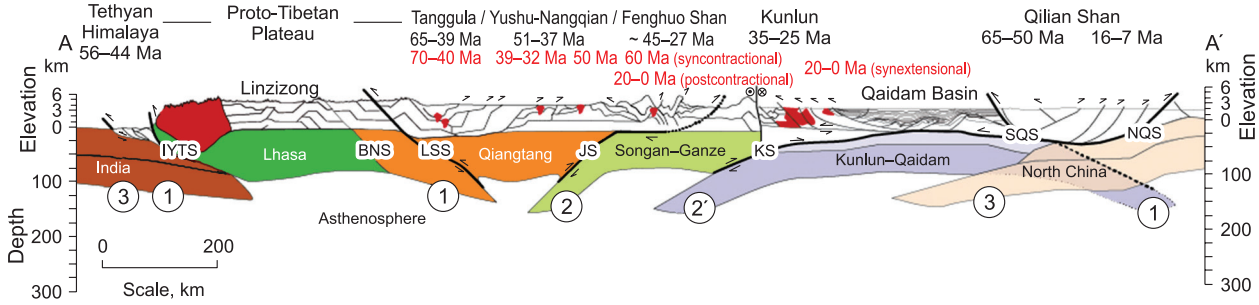

Fig. 16. Schematic cross-section across Tibet supposing reactivation of all the continental slabs through time.

1, Northward continental subduction along the Longmu Co-Shuanghu Suture led to Paleocene deformation and magmatism in the Tanggula Range (Roger et al., 2000; Rohrmann et al., 2012; Wang et al., 2008). Meanwhile, the Himalayan fold-and-thrust belt accommodated the continental subduction of the Indian Plate at the southern edge of the Plateau, the North Qilian suture at its northern edge was reactivated by the southward subduction of the North China lithosphere (Yin et al., 2008). 2, From mid-Eocene to Oligocene, the reactivation of the Jinsha and Kunlun sutures triggered a jump of the deformation northward, to the the Fenghuo Shan and Yushu-Nangqian belts, and resulted in a south-younging syncontractional magmatism from the Fenghuo Shan (Staisch et al., 2014) to the Nangqian basin (Spurlin et al., 2005). 3, In the early Neogene, the deformation was localized at the very southern and northern borders of the plateau, with the activation of the South Tibetan Detachment and main Himalayan thrusts (see synthesis by (Staisch et al., 2016)) and the southward subduction of the North China lithosphere along the North Qilian Shan–Nan Shan suture (Yin et al., 2008). Same legend as Fig. 14.

The continental subduction scenario encounters two main caveats: no Cenozoic reactivation of the Jinsha Suture could be identified with argon geochronometers (Goussin, 2019), and no simple scenario with a single south-directed or north-directed reactivation of a Tibetan suture matches the migration patterns of both the tectonic and magmatic activities across central Tibet (Goussin, 2019). Concerning the absence or the scarcity of Cenozoic thermochronological data recording the crustal thickening, this is a general problem throughout Tibet (Rohrmann et al., 2012; Airaghi et al., 2018b). There is little or no resetting of HT geochronometers. Two complementary processes can explain this observation. Unlike the Himalaya, where the exhumation of deep rocks is accompanied by a strong coupling between tectonic and erosion processes, deep rocks are not exhumed in Tibet due to the absence of erosion processes. Secondly, the thickening of Tibetan crust occurs from below, by underthrusting of crustal material along reactivated suture zones (Meyer et al., 1998; Yin et al., 2008; Replumaz et al., 2016) and consequently, the upper crust was passively uplifted without erosion. This implies a high decoupling at the Proto-Tibetan Moho level (Spurlin et al., 2005; Karplus et al., 2011; Guillot and Replumaz, 2013, Maierová et al., 2016) equivalent to the Main Himalayan Thrust beneath the Himalaya. Moreover, it has been demonstrated by numerical and analog modelling that for a highly buoyant upper mantle, the upper crust cannot support an important horizontal stress and the deformation shifts from localized and planar deformation (mainly oriented thrusting) to homogeneous and horizontal flattening without steep relief formation, the lower crust flows instead laterally (Duclaux et al., 2007; Gapais et al., 2009; Bajolet al., 2013; Pusok and Kaus, 2015). This situation is very similar to the one observed in Central Tibet (Qiangtang and Songpan Ganze) where major intracontinental thrusts are hardly observed and north or south oriented thrusts are only locally recognized (Spurlin et al., 2005, Staitsch et al., 2016).

Assuming a soft Tibetan lithosphere, the total shortening was not accommodated along a single suture zone but by a combination of short-lived intracontinental subduction events and homogeneous deformation (Replumaz et al., 2016), partly overlapping in time, with opposite dips, and with low strain to explain the lack of strong tectonic record at the surface (Guillot and Replumaz, 2013, fig. 16; Goussin, 2019). The timing of the Cenozoic magmatism is a good proxy of the age of the reactivation of the suture zone (Fig. 16). The oldest magmatism is recorded along the Indus and Bangong suture zones suggesting that continental collision initiated here followed by magmatism along the Jinsha suture (2) then Kulun suture (2′). The Qaidam basin records instead no magmatism but a northward propagation of the sedimentation since the Late Cretaceous (Yin et al., 2008, Wu et al., 2016). The Qilian Shan also recorded initiation of deformation during the Late Cretaceous (Clark et al., 2010; Zhang et al., 2018) suggesting a possible earlier (Paleocene) south dipping activation of the North China slab then during the Miocene (3) (Molnar and Stock, 2009).

To summarize, we propose a new three-step scenario for the construction of the Tibetan Plateau (Fig. 17). First, during the Mesozoic, successive accretion of the Gondwana terranes to the southern margin of Eurasia leaded to the formation of the Proto-Tibetan Plateau extending from southern Tibet to the Songpan-Ganze. This

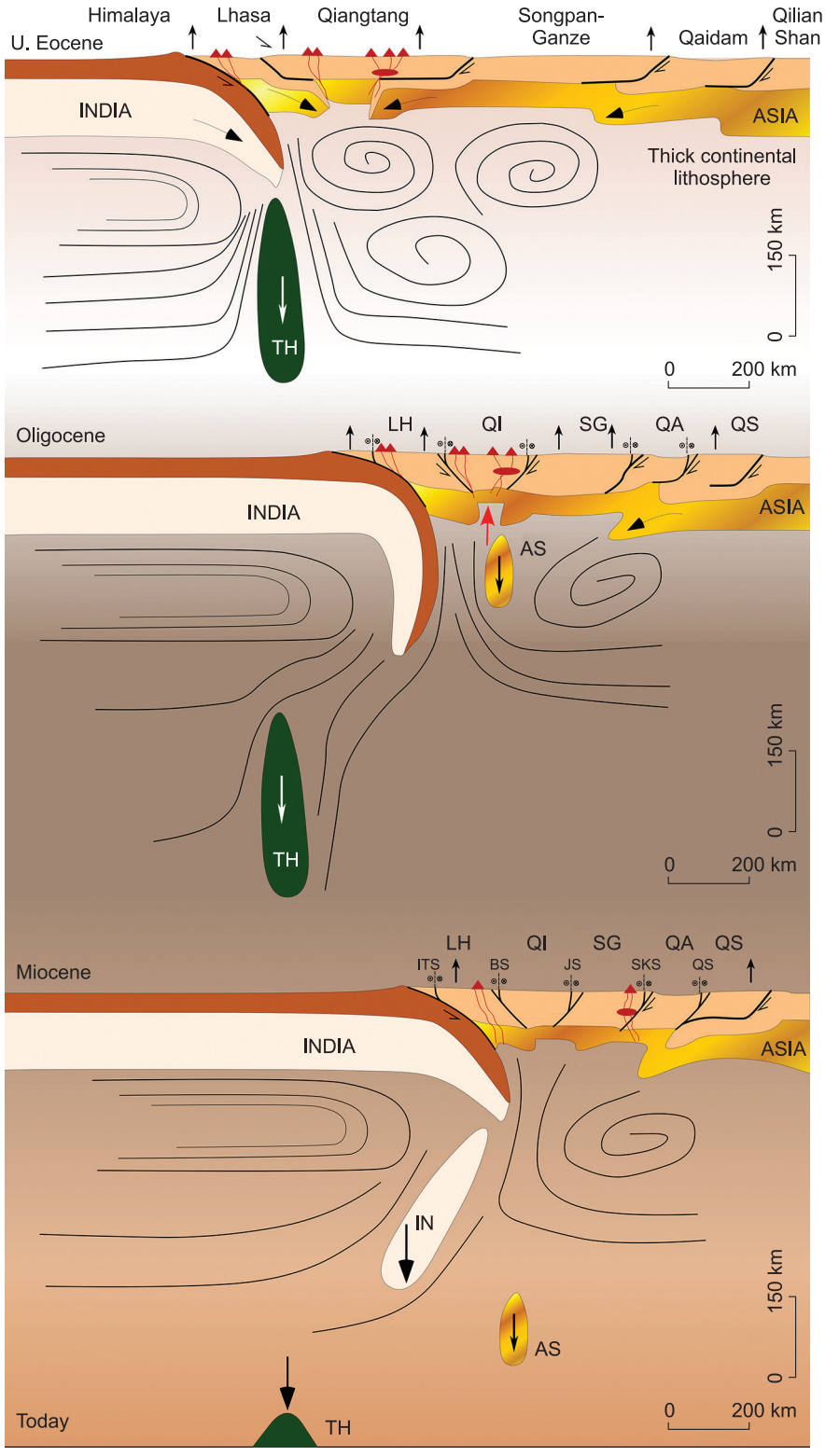

Fig. 17. Schematic evolution of the Himalaya–Tibet orogenic system at the lithospheric scale showing the timing and location of the potassic to utrapotassic magmatism (Guillot and Replumaz, 2013) and the convective cells in the upper mantle (Pitard et al., 2018).

This model takes the tomographic and geophysical data into account, as well as the tectono-metamorphic and magmatic evolution and the estimates of the shortening discussed in the text. LH, Lhasa Block; QI, Qiangtang Block; SG, Songpan–Ganze Block; QA, Qaidam basin; QS, Qilian Shan; TH, Tethyan slab; IN, Indian slab; As, Asian slab.

protoplateau covered a surface of 2/3 of the present-day Tibet, with an average altitude of 2000 to 2500 m. Then, at the onset of the India-Asia collision, the reactivation of the suture zones with underthrusting of crustal material and lithospheric mantle along décollement levels probably at the Moho level resulted in crustal shortening (Bajolet al., 2013; Replumaz et al., 2016), crustal uplift and coeval magmatism. Suture reactivations alternately skipped from the edges to the core of the plateau (Goussin, 2019 and references therein). Finally when the central part of the Tibetan Plateau reached a crustal thickness close to the present one, probably between the late Eocene–early Oligocene, the buoyancy forces becoming higher than the horizontal forces, the deformation propagates outwards of the plateau (Fig. 17). The crustal thickening of the central part of Tibet also triggered the large crustal-scale faulting that lead to the lateral extrusion of Tibet (Tapponnier and Molnar, 1976).

CONCLUSIONS

How and when did the Tibetan Plateau grow? The answer is not trivial as the Tibetan Plateau results from a long-lasting tectonic evolution starting during the early Mesozoic by the accretion of successive continental terranes deriving from Gondwana. In this paper, we show that this 200 Myr-long history characterized by the closure of oceanic domains followed by continental docking had consequences at the lithosphere and crustal scales. At lithospheric mantle level, the successive subductions "polluted" the initial south Asian lithosphere by introducing fluids and metasediments. At crustal level, accretionary prism formation, thickening of the successive basins and magmatic injection in an arc- or Andean-type margin allowed the Proto-Tibetan crust to be thickened. As a consequence, by the late Cretaceous, just before India–Asia collision, a Proto-Tibetan Plateau existed and extended from the Lhasa Block to the Songpan-Ganze, covering between 50% and 75 % of the present-day surface of the Tibetan Plateau, with an average estimated altitude of 2000–2500 m (locally reaching up to 4000 m along reactivated suture zones).

During the India–Asia collision, half of the 2200 km of convergence was accommodated on the Tibetan side. We suppose that the soft metasomatized Tibetan lithosphere accommodated the underthrusting of continental slab by reactivation along or close to the previous intracontinental suture zones. Each slab accommodated limited north–south convergence of a maximum of 100 to 200 km. We suppose that the low seismic velocity zone beneath central Tibet does not correspond to the asthenosphere replacing a delaminated lithosphere but represents the buoyant preserved metasomatized lithosphere. In this scenario, the initial Tibetan lithosphere was squeezed between the Indian slab (at the south), the North China Craton (at the north) and the Sichuan Craton (at the east), while north–south convergence was sustained by far-field forces. This is because the Indian collision is part of a wider convergent system, namely the Tethyan subduction zone, from the Mediterranean to the Banda arc, driving the dynamics of the global system and constraining the force balance at the boundary between India and Eurasia (Pitard et al., 2018). At the crustal level, shortening was accommodated along intracrustal décollements either at mid-crustal level or at the Moho level, preserving the upper crust of strong deformation.

Acknowledgments. The project was made possible by the financial support of Agence Nationale de la Recherche (ANR) AA-PJCJC SIMI5-6 LONGRIBA and ANR-13-BS06-012-01 DSP-Tibet, the INSU-CNRS and Labex "OSUG@2020". We acknowledge Nikolai Sobolev for inviting us to write this paper. The manuscript benefited from insightful comments by Professors N.L. Dobretsov and M.M. Buslov and an anonymous reviewer.

REFERENCES

Airaghi, L., Lanari, P., de Sigoyer, J., Guillot, S., 2017a. Microstructural vs compositional preservation and pseudomorphic replacement of muscovite in deformed metapelites from the Longmen Shan (Sichuan, China). Lithos 282–283, 260–280.

Airaghi, L., de Sigoyer, J., Lanari, P., Guillot, S., Vidal, O., Monié, P. Sautter, B., Tan, X., 2017b. Total exhumation across the Beichuan fault in the Longmen Shan (eastern Tibetan plateau, China): Constraints from petrology and thermobarometry. J. Asian Earth Sci. 140, 108–121.

Airaghi, L., Warren, C.J., de Sigoyer, J., Lanari, P., Magnin, V., 2018a. Influence of dissolution/reprecipitation reactions on metamorphic greenschist to amphibolite facies mica $^{40}Ar/^{39}Ar$ ages in the Longmen Shan (eastern Tibet). J. Metamorph. Geol. 36 (7), 933–958.

Airaghi, L., de Sigoyer, J., Guillot, S., Robert, A., Warren, C.J., Deldicque, D., 2018b. The Mesozoic along-strike tectonometamorphic segmentation of Longmen Shan (Eastern Tibetan Plateau). Tectonics 37 (12), 4655–4678.

Bajolet, F., Replumaz, A., Lainé, R., 2013. Orocline and syntaxes formation during subduction and collision. Tectonics 32 (5), 1529–1546.

Buckman, S., Aitchison, J.C., Nutman, A.P., Bennett, V.C., Saktura, W.M., Walsh, J.M.J., Kachovich, S., Hidaka, H., 2018. The Spongtang Massif in Ladakh, NW Himalaya: An Early Cretaceous record of spontaneous, intra-oceanic subduction initiation in the Neotethys. Gondwana Res. 63, 226–249.

Burg, J.P., Guiraud, M., Chen, G.M., Li, G.C., 1984. Himalayan metamorphism and deformation in the North Himalayan Belt (Southern Tibet, China). Earth Planet. Sci. Lett. 69 (2), 391–400.

Calassou, S., 1994. Etude tectonique d'une chaîne de décollement: Tectonique triasique et tertiaire de la chaîne de Songpan-Garze (east Tibet): Géometrie et cinématique des déformations dans les prismes d'accrétion sédimentaire: Modélisation analogique. PhD Thesis, Université de Montpellier II.

Cheng, Z., Guo, Z., 2017. Post-collisional ultrapotassic rocks and mantle xenoliths in the Sailipu volcanic field of Lhasa terrane, south Tibet: Petrological and geochemical constraints on mantle source and geodynamic setting. Gondwana Res. 46, 17–42.

Chung, S.-L., Chu, M.-F., Zhang, Y., Xie, Y., Lo, C.H., Lee, T.Y., Lan, C.Y., Li, X., Zhang, Q., Wang, Y., 2005. Tibetan tectonic evolution inferred from spatial and temporal variations in post-collisional magmatism. Earth Sci. Rev. 68 (3–4), 173–196.

Clark, M.K., Farley, K.A., Zheng, D., Wang, Z., Duvall, A., 2010. Early Cenozoic faulting of the northern Tibetan Plateau margin from apatite (U–Th)/He ages. Earth Planet. Sci. Lett. 296 (1–2), 78–88.

Cordani, U.G., Milani, E.J., Filho, A.T., Campos, D.A. (Eds.), 2000. Tectonic Evolution of South America. Revista Geológica de Chile.

Dai, J., Zhao, X., Wang, C., Zhu, L., Li, Y., Finn, D., 2012. The vast proto-Tibetan Plateau: New constraints from Paleogene Hoh Xil Basin. Gondwana Res. 22 (2), 434–446.

de Sigoyer, J., Chavagnac, V., Blichert-Toft, J., Villa, I.M., Luais, B., Guillot, S., Cosca, M., Mascle, G., 2000. Dating the Indian continental subduction and collisional thickening in the northwest Himalaya: Multichronology of the Tso Morari eclogites. Geology 28 (6), 487–490.

de Sigoyer, J., Vanderhaeghe, O., Duchêne, S., Billerot, A., 2014. Generation and emplacement of Triassic granitoids within the Songpan Ganze accretionary-orogenic wedge in a context of slab retreat accommodated by tear faulting, Eastern Tibetan plateau, China. J. Asian Earth Sci. 88, 192–216.

DeCelles, P.G., Robinson, D.M., Zandt, G., 2002. Implications of shortening in the Himalayan fold-thrust belt for uplift of the Tibetan Plateau. Tectonics 21 (6), 12-1–12-25

DeCelles, P.G., Kapp, P., Ding, L., Gehrels, G.E., 2007. Late Cretaceous to middle Tertiary basin evolution in the central Tibetan Plateau: Changing environments in response to tectonic partitioning, aridification, and regional elevation gain. GSA Bull. 119 (5–6), 654–680.

Delvaux, D., Cloetingh, S., Beekman F., Sokoutis, D., Burov, E., Buslov, M.M., Abdrakhmatov, K.E., 2013. Basin evolution in a folding lithosphere: Altai–Sayan and Tien Shan belts in Central Asia. Tectonophysics 602, 194–222.

Deng, T., Ding, L., 2015. Paleoaltimetry reconstructions of the Tibetan Plateau: progress and contradictions. Natl. Sci. Rev. 2 (4), 417–437.

Ding, L., Kapp, P., Zhong, D., Deng, W., 2003. Cenozoic volcanism in Tibet: evidence for a transition from oceanic to continental subduction. J. Petrol. 44 (10), 1833–1865.

Ding, L., Kapp, P., Yue, Y., Lai, Q., 2007. Postcollisional calc-alkaline lavas and xenoliths from the southern Qiangtang terrane, central Tibet. Earth Planet. Sci. Lett. 254 (1–2), 28–38.

Dobretsov, N.L., Buslov, M.M., Delvaux, D., Berzin, N.A., Ermikov, V.D., 1996. Meso- and Cenozoic tectonics of the Central Asian mountain belt: effects of lithospheric plate interaction and mantle plumes. Int. Geol. Rev 38, 430–466.

Dobretsov, N.L., Kirdyashkin, A.A., Kirdyashkin, A.G., Vernikovsky, V.A., Gladkov, I.N., 2008. Modelling of thermochemical plumes and implications for the origin of the Siberian traps. Lithos 100 (1–4), 66–92.

Duclaux, G., Rey, P., Guillot, S., Ménot, R.-P., 2007. Orogen-parallel flow during continental convergence: Numerical experiments and Archean field examples. Geology 35 (8), 715–718.

Dupont-Nivet, G., Lippert, P.C., Van Hinsbergen, D., Meijers, M.J.M., Kapp, P., 2010. Palaeolatitude and age of the Indo-Asia collision: palaeomagnetic constraints. Geophys. J. Int. 182 (3), 1189–1198.

Dürr, S. B., 1996. Provenance of Xigaze fore-arc basin clastic rocks (Cretaceous, south Tibet). GSA Bull. 108 (6), 669–684.

Ernst, R.E., Buchan, K.L., 2002. Maximum size and distribution in time and space of mantle plumes: evidence from large igneous provinces. J. Geodyn. 34 (2), 309–342.

Fauquette, S., Clauzon, G., Suc, J.-P., Zheng, Z., 1999. A new approach for palaeoaltitude estimates based on pollen records: example of the Mercantour Massif (southeastern France) at the earliest Pliocene. Earth Planet. Sci. Lett. 170 (1–2), 35–47.

Fauquette, S., Bernet, M., Suc, J.-P., Grosjean, A.-S., Guillot, S., van der Beek, P., Jourdan, S., Popescu, S.-M., Jiménez-Moreno, G., Bertini, A., Pittet, B., Tricart, P., Dumont, T., Schwartz, S., Zheng, Z., Roche, E., Pavia, G., Gardien, V., 2015. Quantifying the Eocene to Pleistocene topographic evolution of the southwestern Alps, France and Italy. Earth Planet. Sci. Lett. 412, 220–234.

Feng, M., An, M., Zhao, W., Xue, G., Mechie, J., Zhao, Y., 2011. Lithosphere structures of northeast Tibetan Plateau and their geodynamic implications. J. Geodyn. 52 (5), 432–442.

Gao, Y., Hou, Z., Kamber, B.S., Wei, R., Meng, X., Zhao, R., 2007. Adakite-like porphyries from the southern Tibetan continental collision zones: evidence for slab melt metasomatism. Contrib. Mineral. Petrol. 153 (1), 105–120.

Gapais, D., Cagnard, F., Gueydan, F., Barbey, F., Ballevre, M., 2009. Mountain building and exhumation processes through time: inferences from nature and models. Terra Nova 21, 188–194.

Ghosh, J., Adkins, H. Affek, B., Balta, B., Guo, W.F., Schauble, E.A., Schrag, D., Eleir, J.M., 2006. ^{13}C-^{18}O bonds in carbonate minerals: A new kind of paleothermometer. Geochim. Cosmochim. Acta 70 (6), 1439–1456.

Glorie, S., De Grave, J., Buslov, M.M., Elburg, M.A., Stockli, D.F., Gerdes, A., Van den Haute, P., 2010. Multi-method chronometric constraints on the evolution of the Northern Kyrgyz Tien Shan granitoids (Central Asian Orogenic Belt): From emplacement to exhumation. J. Asian Earth Sci. 38 (3–4), 131–146.

Glorie, S., De Grave, J., Buslov, M.M., Zhimulev, F.I., Stockli, D.F., Batalev, V.Yu., Izmer, A., Van den Haute, P., Vanhaecke, F., Elburg, M.A., 2011. Tectonic history of the Kyrgyz South Tien Shan (Atbashi-Inylchek) suture zone: The role of inherited structures during deformation-propagation. Tectonics 30 (6), TC6016.

Glorie, S., De Grave, J., Buslov, M.M., Zhimulev, F.I., Elburg, M.A., Van den Haute, P., 2012. Structural control on Meso-Cenozoic tectonic reactivation and denudation in the Siberian Altai: Insights from multi-method thermochronometry. Tectonophysics 544–545, 75–92.

Goussin, F., 2019. Subductions continentales au Tibet Central: héritages pétrologique, rhéologique, et construction d'un plateau. PhD Thesis. Univ. Grenoble Alpes.

Goussin, F., Cordier, C., Boulvais, P., Guillot, S., Roperch, P., Replumaz, A., 2017. Xenoliths in Eocene lavas from Central Tibet record carbonated metasomatism of the lithosphere, in: Proc. Conf. 19th EUG General Assembly (23–28 April 2017, Vienna), p. 4469.

Guillot, S., Mahéo, G., de Sigoyer, J., Hattori, K.H., Pêcher A., 2008. Tethyan and Indian subduction viewed from the Himalayan high- to ultrahigh-pressure metamorphic rocks. Tectonophyics 451 (1–4), 225–241.

Guillot, S., Replumaz, A., 2013. Importance of continental subductions for the growth of the Tibetan plateau. Bull. Soc. Géol. France 184 (3), 199–223.

Guo, Z., Wilson, M., Liu, M., Mao, Q., 2006. Post-collisional, potassic and ultrapotassic magmatism of the Northern Tibetan Plateau constraints on characteristics of the mantle source, geodynamic setting and uplift mechanisms. J. Petrol. 47 (6), 1177–1220.

Guynn, J., Kapp, P., Gehrels, G.E., Ding, L., 2012. U–Pb geochronology of basement rocks in central Tibet and paleogeographic implications. J. Asian Earth Sci. 43 (1), 23–50.

Hébert, R., Bezard, R., Guillemette, C., Dostal, J., Wang, C.S., Liu, Z.F., 2012. The Indus–Yarlung Zangbo ophiolites from Nanga Parbat to Namche Barwa syntaxes, southern Tibet: First synthesis of petrology, geochemistry and geochronology with incidences on geodynamic reconstructions of Neo-Tethys. Gondwana Res. 22 (2), 377–397.

Horton, B.K., Yin, A., Spurlin, M.S., Zhou, J., Wang, J., 2002. Paleocene–Eocene syncontractional sedimentation in narrow, lacustrine-dominated basins of east-central Tibet. GSA Bull. 114 (7), 771–786.

Jiménez-Munt, I., Platt, J.P., 2006. Influence of mantle dynamics on the topographic evolution of the Tibetan Plateau: Results from numerical modeling. Tectonics 25 (6), TC6002.

Jolivet, M., 2017. Mesozoic tectonic and topographical evolution of Central Asia and Tibet: a preliminary synthesis, in: Brunet, M.-F., McCann, T., Sobel, E.R. (Eds.), Geological Evolution of Central Asian Basins and the Western Tien Shan Range. Geol. Soc. London, Spec. Publ. 427, pp. 19–55.

Kapp, P., Yin, A., Manning, C.E., Harrison, T.M., Taylor, M.H., Lin, D., 2003. Tectonic evolution of the early Mesozoic blueschist-bearing Qiangtang metamorphic belt, central Tibet. Tectonics 22 (4), 1043.

Kapp, P., Yin, A., Harrison, T.M., Ding, L., 2005. Cretaceous-Tertiary shortening, basin development, and volcanism in central Tibet. GSA Bull. 117 (7–8), 865–878.

Kapp, P., DeCelles, P.G., Gehrels, G.E., Heizler, M., Ding, L., 2007. Geological records of the Lhasa-Qiangtang and Indo-Asian collisions in the Nima area of central Tibet. GSA Bull. 119 (7–8), 917–933.

Karplus, M. S., Zhao, W., Klemperer, S.L., Wu, Z., Mechie, J., Shi, D., Brown, L.D., Chen, C., 2011. Injection of Tibetan crust beneath the south Qaidam Basin: Evidence from INDEPTH IV wide-angle seismic data. J. Geophys. Res. Solid Earth 116 (B7), B07301.

Kind, R., Yuan, X., Saul, J., Nelson, D., Sobolev, S.V., Mechie, J., Zhao, W., Kosarev, G., Ni, J., Achauer, U., Jiang, M., 2002. Seismic images of crust and upper mantle beneath Tibet: Evidence for Eurasian plate subduction. Science 298 (5596), 1219–1221.

Kirby, E., Reiners, P.W., Krol, M.A., Whipple, K.X., Hodges, K.V., Farley, K.A., Tang, W., Chen, Z., 2002. Late Cenozoic evolution of the eastern margin of the Tibetan Plateau: Inferences from $^{40}Ar/^{39}Ar$ and (U–Th)/He thermochronology. Tectonics 21 (1), 1-1–1-20.

Koulakov, I., Sobolev, S.V., 2006. A tomographic image of Indian lithosphere break-off beneath the Pamir–Hindukush region. Geophys. J. Int.164 (2), 425–440.

Lai, S.C., Qin, J.F., Khan, J., 2014. The carbonated source region of Cenozoic mafic and ultra-mafic lavas from western Qinling: Implications for eastern mantle extrusion in the northeastern margin of the Tibetan Plateau. Gondwana Res. 25 (4), 1501–1516.

Li, G.M., Qin, K.Z., Li, J.X., Evans, N.J., Zhao, J.X., Cao, M.J., Zhang, X.N., 2017. Cretaceous magmatism and metallogeny in the Bangong –Nujiang metallogenic belt, central Tibet: Evidence from petrogeochemistry, zircon U–Pb ages, an Hf–O isotopic compositions. Gondwana Res. 41, 110–127.

Li, L., Fan, M., Davila, N., Jesmok, G., Mitsunaga, B., Tripati, A., Orme, D., 2019. Carbonate stable and clumped isotopic evidence for late Eocene moderate to high elevation of the east-central Tibetan Plateau and its geodynamic implications. GSA Bull. 131 (5–6), 831–844.

Liang, C., Song, X., 2006. A low velocity belt beneath northern and eastern Tibetan Plateau from Pn tomography. Geophys. Res. Lett. 33 (22), L22306.

Liu, G.-Z., Wu, F.-Y., Chung, S.-L., Zhao, Z.-D., 2011. Fragments of hot and metasomatized mantle lithosphere in Middle Miocene ultrapotassic lavas, southern Tibet. Geology 39 (10), 923–926.

Mahéo, G., Guillot, S., Blichert-Toft, Y., Rolland, Y., Pêcher A., 2002. A slab breakoff model for the Neogene thermal evolution of South Karakorum and South Tibet. Earth Planet. Sci. Lett. 195 (1–2), 45–58.

Mahéo, G., Bertrand, H., Guillot, S., Villa, I.M., Keller, F., Capiez, P., 2004. The South Ladakh ophiolites (NW Himalaya, India): an intra-oceanic tholeiitic arc origin with implications for the closure of the Neo-Thethys. Chem. Geol. 203 (3–4), 273–303.

Maierová, P., Schulmann, K., Lexa, O., Guillot, S., Štípská, P., Janoušek, V., Cadek, O., 2016. European Variscan orogenic evolution as an analogue of Tibetan-Himalayan orogen: Insights from petrology and numerical modeling. Tectonics 35 (7), 1760–1780.

Marcoux, J., Girardeau, J., Fourcade, E., Bassoullet, J.P., Philip J., Jaffrezo, M., Xuchan, X., Cheng, C. 1987. Geology and biostratigraphy of the Jurassic and Lower Cretaceous series to the north of the Lhasa Block (Tibet, China). Geodin. Acta 1 (4–5), 313–325.

Maruyama, Sh., 1994. Plume tectonics. J. Geol. Soc. Japan 100, 24–49.

Métivier, F., Gaudemer, Y., Tapponnier, P., Meyer, B., 1998. Northeastward growth of the Tibet plateau deduced from balanced reconstruction of two depositional areas: The Qaidam and Hexi Corridor basins, China. Tectonics 17 (6), 823–842.

Meyer, B., Tapponnier, P., Bourjot, L., Métivier, F., Gaudemer, Y., Peltzer, G., Shunmin, G., Zhitai, C., 1998. Crustal thickening in Gansu-Qinghai, lithospheric mantle subduction, and oblique, strike-slip controlled growth of the Tibet plateau. Geophys. J. Int. 135 (1), 1–47.

Miller, C., Schuster, R., Klötzli, U., Frank, W., Purtscheller, F., 1999. Post-collisional potassic and ultrapotassic magmatism in SW Tibet: geochemical and Sr–Nd–Pb–O isotopic constraints for mantle source characteristics and petrogenesis. J. Petrol. 40 (9), 1399–1424.

Molnar, P., 1988. A review of geophysical constraints on the deep structure of the Tibetan Plateau, the Himalaya and the Karakoram, and their tectonic implications. Phil. Trans. Soc. London A 326 (1589). DOI: 10.1098/rsta.1988.0080.

Molnar, P., Stock, J.M., 2009. Slowing of the India's convergence with Eurasia since 20 Ma and its implications for Tibtean mantle dynamics. Tectonics 28 (3), TC3001.

Molnar, P., Tapponnier P., 1975. Cenozoic tectonics of Asia: Effects of a continental collision. Science 189, 419–426.

Molnar, P., England, P., Martinod, J., 1993. Mantle dynamics, uplift of the Tibetan Plateau, and Indian monsoon. Rev. Geophys. 31 (4), 357–396.

Murphy, M.A., Yin, A., Harrison, T.M., Dürr, S.B., Chen, Z., Ryerson, F.J., Kidd, W.S.F., Wang, X., Zhou, X., 1997. Did the Indo-Asian collision alone create the Tibetan plateau? Geology 25 (8), 719–722.

Nunn, C., Roecker, S.W., Priestley, K.F., Liang, X., Gilligan, A., 2014. Joint inversion of surface waves and teleseismic body waves across the Tibetan collision zone: The fate of subducted Indian lithosphere. Geophys. J. Int. 198 (3), 1526–1542.

Peccerillo. A., 2004. Carbonate-rich pyroclastic rocks from central Apennines: Carbonatites or carbonated rocks? A commentary. Periodico di Mineralogia 73, 165–175.

Pitard, P., Replumaz, A., Funiciello, F., Husson, L., Faccenna, C., 2018. Mantle kinematics driving collisional subduction: Insights from analogue modeling. Earth Planet. Sci. Lett. 502, 96–103.

Price, R.A., 1981. The Cordilleran foreland thrust and fold belt in the southern Canadian Rocky Mountains. Geol Soc. London, Spec. Publ. 9, 427–448.

Priestley, K., McKenzie, D., 2006. The thermal structure of the lithosphere from shear wave velocities. Earth Planet. Sci. Lett. 244 (1–2), 285–301.

Priestley, K., McKenzie, D., 2013. The relationship between shear wave velocity, temperature, attenuation and viscosity in the shallow part of the mantle. Earth Planet. Sci. Lett. 381, 78–91.

Priestley, K., Debayle, E., McKenzie, D., Pilidou, S., 2006. Upper mantle structure of eastern Asia from multimode surface waveform tomography. J. Geophys. Res. Solid Earth 111 (B10), B10304.

Pullen, A., Kapp, P., Gehrels, E., Ding, L., Zhang, Q., 2011. Metamorphic rocks in central Tibet: Lateral variations and implications for crustal structure. GSA Bull. 123 (3–4), 585–600.

Pusok, A.E., Kaus, B.J., 2015. Development of topography in 3-D continental-collision models. Geochem. Geophys. Geosyst. 16 (5), 1378–1400.

Replumaz, A., Negredo, A.M., Villasenor, A., Guillot, S., 2010. Indian continental subduction and slab break-off during Tertiary collision. Terra Nova 22 (4), 290–296.

Replumaz, A., Capitanio, F.A., Guillot, S., Negredo, A.M., Villaseñor, A., 2014. The coupling of Indian subduction and Asian continental tectonics. Gondwana Res. 26 (2), 608–626.

Replumaz, A., Funiciello, F., Reitano, R., Faccenna, C., Balon, M., 2016. Asian collisional subduction: A key process driving formation of the Tibetan Plateau. Geology 44 (11), 943–946.

Roger, F., Tapponnier, P., Arnaud, N., Schärer, U., Brunel, M., Zhiqin, X., Jingsui, Y., 2000. An Eocene magmatic belt across central Tibet: mantle subduction triggered by the Indian collision. Terra Nova 12 (3), 102–108.

Roger, F., Jolivet, M., Malavieille, J., 2010. The tectonic evolution of the Songpan-Garzê (North Tibet) and adjacent areas from Proterozoic to Present: a synthesis. J. Asian Earth Sci. 39 (4), 254–269.

Rohrmann, A., Kapp, P., Carrapa B., Reiners, P., Guynn, J., Ding, L., Heizler, M., 2012. Thermochronologic evidence for plateau formation in central Tibet by 45 Ma. Geology 40 (2), 187–190.

Rohrmann, A., Barbolini, N., Meijer, N., Yang, Z., Dupont-Nivet, G., 2018. High Central Tibet at the onset of Indo-Asian collision derived from leaf-wax hydrogen and palynology data, in: Hetényi, G., Guillermin, Z., Jordan, M., Raymond, G., Subedi, S., Buchs, N., Robyr, M., Epard, J.L. (Eds.), Abstract Volume of the 33rd Himalaya–Karakorum–Tibet Workshop (10–12 September 2018, Lausanne), p. 143. Lausanne.

Searle, M.P., Tirrul, R., 1991. Structural and thermal evolution of the Karakorum crust. J. Geol. Soc. 148, 65–82.

Sobel, E.R., Osnik, M., Burbank, D., Mikolaichuk, A., 2006. Exhumation of basement-cored uplifts: example of the Kyrgyz Range quantified with apatite fission track thermochronology. Tectonics 25 (2), TC2008.

Spurlin, M.S., Yin, A., Horton, B.K., Zhou, J., Wang, J., 2005. Structural evolution of the Yushu-Nangqian region and its relationship to syncollisional igneous activity, east-central Tibet. GSA Bull. 117 (9–10) 1293–1317.

Staisch, L.M., Niemi, N.A., Chang, H., Clark, M.K., Rowley, D.B., Currie, B.S., 2014. A Cretaceous–Eocene depositional age for the Fenghuoshan Group, Hoh Xil Basin: Implications for the tectonic evolution of the northern Tibet Plateau. Tectonics 33 (3), 281–301.

Staisch, L.M., Niemi, N.A., Clark, M.K., Chang, H., 2016. Eocene to late Oligocene history of crustal shortening within the Hoh Xil Basin and implications for the uplift history of the northern Tibetan Plateau. Tectonics 35 (4), 862–895.

Stepanov, A.S., Campbell, I., Rapp, R.P., Lowczak, J., Korsakov, A.V., 2017. Discussion: "Xenoliths in ultrapotassic volcanic rocks in the Lhasa block: Direct evidence for crust–mantle mixing and metamorphism in the deep crust" by Wang et al. 2016 (Contributions to Mineralogy and Petrology) 171: 62. Contrib. Mineral. Petrol. 172: 19. DOI: 10.1007/s00410-017-1332-6.

Tapponnier, P., Molnar, P., 1976. Slip-line field theory and large-scale continental tectonics. Nature 264 (5584), 319–324.

Tapponnier, P., Zhiqin, X., Roger, F., Meyer, B., Arnaud, N., Wittlinger, G., Jingsui, Y., 2001. Oblique stepwise rise and growth of the Tibetan Plateau. Science 294 (5547), 1671–1677.

Tunini, L., Jiménez-Munt, I., Fernandez, M., Vergés, J., Villaseñor, A., Melchiorre, M., Afonso, J.C., 2016. Geophysical-petrological model of the crust and upper mantle in the India–Eurasia collision zone. Tectonics 35 (7) 1642–1669.

Turner, S., Arnaud, N., Liu, J., Rogers, N., Hawkesworth, C., Harris, N., Kelley, S., Van Calsteren, P., Deng, W., 1996. Post-collision, shoshonitic volcanism on the Tibetan Plateau: implications for convective thinning of the lithosphere and source of Ocean Island Basalt. J. Petrol. 37 (1), 45–71.

Van der Voo, R., Spakman, W., Bijwaard, H., 1999. Tethyan subducted slabs under India. Earth Planet. Sci. Lett. 171 (1), 7–20.

Vozar, J., Jones, A.G., Fullea, J., Agius, M.R., Lebedev, S., Le Pape, F., Wei, W., 2014. Integrated geophysical-petrological modeling of lithosphere–asthenosphere boundary in central Tibet using electromagnetic and seismic data. Geochem. Geophys. Geosyst. 5 (10), 3965–3988.

Wang, C., Zhao, X., Liu, Z., Lippert, P.C., Graham, S.A., Coe, R.S., Yi, H., Zhu, L., Liu, S., Li, Y., 2008. Constraints on the early uplift history of the Tibetan Plateau. PNAS 105 (13), 4987–4992.

Wang, C., Dai, J., Zhao, X., Li, Y., Graham, S.A., He, D., Ran, B., Meng, J., 2014. Outward-growth of the Tibetan Plateau during the Cenozoic: A review. Earth Sci. Rev. 621, 1–43.

Wang, C., Ding, L., Zhang, L.Y., Kapp, P., Pullen, A., Yue, Y.H., 2016. Petrogenesis of Middle–Late Triassic volcanic rocks from the Gangdese belt, southern Lhasa terrane: Implications for early subduction of Neo-Tethyan oceanic lithosphere. Lithos 262, 320–333.

Wang, E., Xu, F.Y., Zhou, J.X., Wan, J., Burchfiel, B.C., 2006. Eastward migration of the Qaidam basin and its implications for Cenozoic evolution of the Altyn Tagh fault and associated river systems. GSA Bull. 118 (3–4), 349–365.

Wang, R., Collins, W.J., Weinberg, R.F., Li, J.X., Li, Q.Y., He, W.Y., Richards, J.P., Hou, Z., Zhou, L.M., Stern, R.A., 2016. Xenoliths in ultrapotassic volcanic rocks in the Lhasa block: Direct evidence for crust–mantle mixing and metamorphism in the deep crust. Contrib. Mineral. Petrol. 171: 62. DOI: 10.1007/s00410-016-1272-6.

Wu, H., Li, C., Chen, J., Xie, C., 2016. Late Triassic tectonic framework and evolution of Central Qiangtang, Tibet, SW China. Lithosphere 8 (2) 141–149.

Xu, C., Huang, Z., Liu, C., Qi, L., Li, W., Guan, T., 2003. Geochemistry of carbonatites in Maoniuping REE deposit, Sichuan province, China. Sci. China Series D: Earth Sci. 46 (3), 246–256.

Xu, C., Chakhmouradian, A.R., Taylor, R.N., Kynicky, J., Li, W., Song, W., Fletcher, I.R., 2014. Origin of carbonatites in the South Qinling orogen: Implications for crustal recycling and timing of collision between the South and North China Blocks. Geochim. Cosmochim. Acta 143, 189–206.

Xue, Z., Martelet, G., Lin, W., Faure, M., Chen, Y., Wei, W., Li, S., Wang, Q., 2017. Mesozoic crustal thickening of the Longmenshan Belt (NE Tibet, China) by imbrication of basement slices: Insights from structural analysis, petrofabric and magnetic fabric studies, and gravity modeling. Tectonics 36 (12), 3110–3134.

Yang, J., Xu, Z., Li, Z., Xu, X., Li, T., Ren, Y., Li, H., Chen, S., Robinson, P.T., 2009. Discovery of an eclogite belt in the Lhasa block, Tibet: A new border for Paleo-Tethys? J. Asian Earth Sci. 34 (1), 76–89.

Yang, J.S., Robinson, P.T., Jiang, C.F., Xu, Z.Q., 1996. Ophiolites of the Kunlun Mountains, China and their tectonic implications. Tectonophysics 258 (1–4), 215–231.

Yang, T., Ding, Y., Zhang, H., Fan, J., Liang, M., Wang. X, 2014. Two-phase subduction and subsequent collision defines the Paleotethyan tectonics of the southeastern Tibetan Plateau: Evidence from zircon U–Pb dating, geochemistry, and structural geology of the Sanjiang orogenic belt, southwest China. Geol. Soc. Am. 126 (11–12), 1654–1682.

Yang, Z., Woolley, A., 2006. Carbonatites in China: A review. J. Asian Earth Sci. 27 (5), 559–575.

Yin, A., Harrison, T.M., 2000. Geologic evolution of the Himalayan–Tibetan orogeny. An. Rev. Earth Planet. Sci. 28, 211–280.

Yin, A., Dang, Q., Chen, X.H., McRivette, M.W., 2008. Cenozoic tectonic evolution of the Qaidam basin and its surrounding regions (Part 3): Structural geology, sedimentation, and regional tectonic reconstruction. GSA Bull. 120 (7–8), 847–876.

Zhang, H.R., Yang, T.N., Hou, Z.Q., Song, Y.C., Ding, Y., Cheng, X.F., 2013. Petrogenesis and tectonics of late Permian felsic volcanic rocks, eastern Qiangtang block, north-central Tibet: Sr and Nd isotopic evidence. Int. Geol. Rev. 55 (8), 1017–1028.

Zhang, H., Yang, T., Hou, Z., Dai, M., Hou, K., 2017. Permian back-arc basin basalts in the Yushu area: New constrain on the Paleo-Tethyan evolution of the north-central Tibet. Lithos 286–287, 216–226.

Zhang, X.Z., Dong, Y.S., Wang, Q., Dan, W., Zhang, C., Deng, M.R., Xu, W., Xia, X.P., Zeng, J.P., Liang, H., 2016. Carboniferous and Permian evolutionary records for the Paleo-Tethys Ocean constrained by newly discovered Xiangtaohu ophiolites from central Qiangtang, central Tibet. Tectonics 35 (7), 1670–1686.

Zhang, Y.X., Jin, X., Zhang, K.J., Sun, W.D., Liu, J.M., Zhou, X.Y., Yan, L.L., 2018. Newly discovered Late Triassic Baqing eclogite in central Tibet indicates an anticlockwise West–East Qiangtang collision. Sci. Rep. 8 (1): 966.

Zhang, Zh., Teng, J., Romanelli, F., Braitenberg, C., Ding, Z., Zhang, X., Fang, L., Zhang, S., Wu, J., Deng, Y., Ma, T., Sun, R., Panza, G.P., 2014. Geophysical constraints on the link between cratonization and orogeny: Evidence from the Tibetan Plateau and the North China Craton. Earth Sci. Rev. 130, 1–48.

Zhao, J., Yuan, X., Liu, H., Kumar, P., Pei, S., Kind, R., Zhang, Z., Teng, J., Ding, L., Gao, X., Xu, Q., Wang, W., 2010. The boundary between the Indian and Asian tectonic plates below Tibet. PNAS 107, 11,229–11,233.

Zhao, W., Kumar, P., Mechie, J., Kind, R., Meissner, R., Wu, Z., Shi, D., Su, H., Xue, G., Karplus, M., Tilmann, F., 2011. Tibetan plate overriding the Asian plate in central and northern Tibet. Nature Geosci. 4 (12), 870–873.

Zhu, D.C., Zhao, Z.D., Dilek, Y., Mo, X.X., 2011. Lhasa terrane in southern Tibet came from Australia. Geology 39 (8), 727–730.

Zhu, D.-C., Zhao, Z.D., Niu, Y., Mo, X.X., Chung, S.L., Hou, Z.Q., Wang, L.Q., Wu, F.Y., 2016. The Lhasa Terrane: Record of a microcontinent and its histories of drift and growth. Earth Planet. Sci. Lett. 301 (1–2), 241–255.

Zhu, D.-C., Wang, Q., Cawood, P.A., Zhao, Z.D., Mo, X.X., 2017. Raising the Gangdese Mountains in southern Tibet. J. Geophys. Res. 122 (1), 214–223.

Рекомендована к печати 22 мая 2019 г.
Н.В. Соболевым

Поступила в редакцию
11 февраля 2019 г.